Available online at www.sciencedirect.com

SciVerse ScienceDirect

PHOTONICS AND NANOSTRUCTURES Fundamentals and Applications

Photonics and Nanostructures – Fundamentals and Applications 11 (2013) 374–396

www.elsevier.com/locate/photonics

Homogenization of spatially dispersive metamaterial arrays in terms of generalized electric and magnetic polarizations

Arthur D. Yaghjian [a,*], Andrea Alù [b], Mário G. Silveirinha [c]

[a] Electromagnetics Research Consultant, 115 Wright Road, Concord, MA 01742, USA

[b] Department of Electrical & Computer Engineering, The University of Texas, Austin, TX 78712, USA

[c] Department of Electrical Engineering-Instituto de Telecomunicações, University of Coimbra, Coimbra, Portugal

Received 26 January 2013; received in revised form 12 March 2013; accepted 15 April 2013

Available online 29 April 2013

Abstract

An anisotropic homogenization theory for spatially dispersive periodic arrays is developed, based on the microscopic Maxwell equations, that yields causal, macroscopic permittivities, and inverse permeabilities for the fundamental Floquet modes of the arrays. (Macroscopic magnetoelectric coefficients are not required.) Reality conditions, reciprocity relations, passivity conditions, and causality relations are derived for these spatially dispersive macroscopic constitutive parameters. A significant feature of the formulation is that the macroscopic permittivities and permeabilities reduce to their anisotropic-continuum definitions in terms of ordinary macroscopic averages at the low spatial and temporal frequencies. In addition, diamagnetic metamaterial arrays require no special considerations or modifications to accommodate their unusual characteristics. A numerical example of a 2D array comprised of circular–cylinder inclusions is given that confirms the theoretical results for the computed electric and magnetic or diamagnetic macroscopic polarizations.

Keywords: Maxwell's equations; Spatial dispersion; Metamaterial arrays; Homogenization; Anisotropy

1. Introduction

As motivation for this work, consider the difficulties encountered in dealing with a diamagnetic array, in particular, a 3D cubic periodic array of perfectly electrically conducting (PEC) spheres in free space. When this array is described by a spatially nondispersive dipolar continuum, it has a macroscopic permittivity $\epsilon(\omega)$ and a macroscopic permeability $\mu(\omega)$, which are functions of frequency ω. Assume that a dipolar homogenization procedure exists for determining a causal $\epsilon(\omega)$ and $\mu(\omega)$ for this PEC-sphere array. Since both the electric and magnetic dipole moments of PEC spheres in a source-free incident field approach zero as $\omega\to\infty$, we also have that $\epsilon(\omega)\to\epsilon_0$ and $\mu(\omega)\to\mu_0$ as $\omega\to\infty$ where ϵ_0 and μ_0 are the permittivity and permeability of free space. Consequently, the causal functions $[\epsilon(\omega)-\epsilon_0]$ and $[\mu(\omega)-\mu_0]$ should obey the Kramers–Kronig relations written in compact form as [1, p. 98]

$$\epsilon(\omega)-\epsilon_0=\frac{i}{\pi}\int_{-\infty}^{+\infty}\frac{\epsilon(\nu)-\epsilon_0}{\omega-\nu}d\nu \tag{1a}$$

$$\mu(\omega)-\mu_0=\frac{i}{\pi}\int_{-\infty}^{+\infty}\frac{\mu(\nu)-\mu_0}{\omega-\nu}d\nu\,. \tag{1b}$$

* Corresponding author. Tel.: +1 978 369 4136.
E-mail address: a.yaghjian@comcast.net (A.D. Yaghjian).

1569-4410/$ – see front matter © 2013 Elsevier B.V. All rights reserved.
http://dx.doi.org/10.1016/j.photonics.2013.04.001

Passivity in a spatially nondispersive dipolar continuum also demands that [1, p. 96]

$$\omega\,\mathrm{Im}[\epsilon(\omega)] \geq 0 \tag{2a}$$

$$\omega\,\mathrm{Im}[\mu(\omega)] \geq 0\,. \tag{2b}$$

The expressions in (1a) and (2a), and in (1b) and (2b), can be combined to prove that

$$\epsilon(0) \geq \epsilon_0 \tag{3a}$$

$$\mu(0) \geq \mu_0 \tag{3b}$$

under the assumptions that the imaginary parts of $\epsilon(\omega)$ and $\mu(\omega)$ are negligible in the neighborhood of $\omega = 0$ and that $\omega d\epsilon(\omega)/d\omega$ and $\omega d\mu(\omega)/d\omega$ both $\to 0$ as $\omega \to 0$ [2, sec. 84], [3]—assumptions satisfied by the $\epsilon(\omega)$ and $\mu(\omega)$ of the PEC-sphere array. The inequality for permittivity in (3a) is certainly obeyed by the 3D array of PEC spheres. However, the inequality for permeability in (3b) is clearly violated by the PEC sphere array, which is strongly diamagnetic [4, sec. 9.5], [5, fig. 8] at low frequencies and thus has $\mu(0) < \mu_0$.

This apparent paradox can be explained by noting that we are assuming that the array behaves as a spatially nondispersive dipolar continuum for all frequencies ω. In fact, as the frequency increases, the electromagnetic properties of the array can no longer be described by macroscopic Maxwellian equations for a spatially nondispersive continuum characterized by dipolar $\epsilon(\omega)$ and $\mu(\omega)$ that necessarily satisfy the causality relations in (1) or the passivity conditions in (2) [6]. In the case of the PEC spheres, this inadequacy of a spatially nondispersive continuum description of the array at higher frequencies is manifested in part by the paradoxical conclusion that $\mu(0) \geq \mu_0$. In particular, it is impossible for a function $\mu(\omega)$ or $\mu^{-1}(\omega)$ to satisfy the Kramers–Kronig causality relations (given in (1b) for $\mu(\omega)$) and the passivity condition in (2b) if $\mu(\omega)$ or $\mu^{-1}(\omega)$ is real and continuously differentiable near $\omega = 0$ and $\mu(0) < \mu_0$. Moreover, using a bianisotropic description of the PEC-sphere array and expanding the induced fields of the array with higher-order multipole moments, while maintaining a spatially nondispersive continuum description of the array, allow additional constitutive parameters but still require a diamagnetic $\mu(\omega)$ with $\mu(0) < \mu_0$ that violates the Kramers–Kronig causality relations for $\mu(\omega)$ or $\mu^{-1}(\omega)$.

Consequently, to adequately describe a 3D array in a way that reduces at lower spatial and temporal frequencies to a continuum description in terms of permittivity and permeability, we proceed to formulate an anisotropic representation for 3D periodic arrays that rigorously takes into account spatial as well as temporal dispersion. We show that such a formulation automatically produces a macroscopic permittivity and inverse permeability that satisfy causality and are free of inconsistencies even if the array exhibits diamagnetism.

Most homogenization theories in the past have been formulated for source-free arrays in which the propagation vectors $\boldsymbol{\beta}$ are functions of the frequency ω [7–10], and we refer to these papers and their references for an overview of the subject. However, to fully characterize the effects of spatial dispersion in plasmas and crystals, Landau and Lifshitz [2, ch. 12], Silin and Rukhadze [11], and Agranovich and Ginzburg [12] decompose the fields and sources of a spatially dispersive, homogeneous continuum into a spectrum of $e^{i(\boldsymbol{\beta}\cdot\mathbf{r}-\omega t)}$ plane waves, where $\boldsymbol{\beta}$ is a real propagation vector and ω is a real angular frequency. These authors combine all electric and magnetic polarization effects (including all multipoles) into a single electric-magnetic polarization density $\mathbf{P}_L(\boldsymbol{\beta}, \omega)$ (based on a single microscopic electric current density induced by an applied electric current density). They then assign a single permittivity dyadic $\overline{\boldsymbol{\epsilon}}_L(\boldsymbol{\beta}, \omega)$ to the single polarization vector such that $\mathbf{P}_L(\boldsymbol{\beta}, \omega) = [\overline{\boldsymbol{\epsilon}}_L(\boldsymbol{\beta}, \omega) - \epsilon_0\overline{\mathbf{I}}] \cdot \mathbf{E}(\boldsymbol{\beta}, \omega)$, where $\mathbf{E}(\boldsymbol{\beta}, \omega)$ is the electric field and $\overline{\mathbf{I}}$ is the unit dyadic. Agranovich and Ginzburg [12, ch. 3] discuss the conditions under which this continuum formulation applies to the fundamental Floquet mode of a natural crystal lattice. More recently, Silveirinha [13–15] has extended and applied the single-polarization formulation to 2D and 3D periodic metamaterial arrays.

Although the single-polarization formulation for a continuum [2,11,12] and periodic metamaterials [13–15] is both accurate and elegant, and has the advantage of an appealing simplicity for many applications, it has some disadvantages as well. For instance, practical solutions to the Maxwellian microscopic equations for metamaterial arrays are commonly developed by separately determining electric and magnetic polarizations, whether or not the two polarizations are eventually combined. Moreover, the $\overline{\boldsymbol{\epsilon}}_L(\boldsymbol{\beta}, \omega)$ dyadic for the single polarization does not reduce to a scalar even if the medium is an isotropic continuum and, thus, in reality it requires no fewer unknowns than the conventional formulation that uses both electric and magnetic polarizations. The single-polarization formulation is especially awkward for dealing with inclusions that produce significant macroscopic magnetization effects in periodic arrays, and it does not provide a definitive prescription for determining causal permittivity and permeability dyadics from the

single-polarization dyadic $\overline{\boldsymbol{\epsilon}}_L(\boldsymbol{\beta},\omega)$, although recipes for determining approximate permittivities and permeabilities from the single polarization have been given in [13].

To help alleviate the drawbacks of the single-polarization approach, Fietz and Shvets [16] introduce applied magnetic current density in addition to applied electric current density and approximate macroscopic averages in such a way that certain boundary integrals of the microscopic and macroscopic fields over the unit cells are equal in order to formulate a spatially dispersive macroscopic bianisotropic representation of metamaterials. In this bianisotropic formulation, they find that, even with nonbianisotropic, centrosymmetric inclusions, a lattice bianisotropy [17] can be induced for $\boldsymbol{\beta} \neq 0$. Alù [18] has developed a straightforward spatially dispersive bianisotropic representation for periodic metamaterials with applied electric and magnetic current densities by expanding the induced electric and magnetic polarization densities with a multipole power series in the propagation vector $\boldsymbol{\beta}$. In Alù's formulation, weak spatial dispersion effects may be properly assigned to local bianisotropic parameters that allow a physically meaningful homogenized description of the array in the limit of low spatial and temporal frequencies. Also, this description does not depend on whether the driving currents are electric, magnetic, or both.

General reciprocity relations, passivity conditions, and causality relations have not been determined for spatially dispersive bianisotropic constitutive parameters in either [16] or [18], and these relationships are not necessarily the same as those in a spatially nondispersive continuum.

1.1. Outline of the paper

In the present work, we excite 3D periodic arrays with an applied plane-wave $e^{i(\boldsymbol{\beta}\cdot\mathbf{r}-\omega t)}$ electric current density only, and decompose the induced electric current density into generalized electric and magnetic polarization densities that maintain the Maxwellian representation for the fundamental Floquet modes of the 3D periodic, spatially dispersive metamaterial arrays comprised of general lossy or lossless polarizable inclusions electrically separated in free space. We show that, within this decomposition, anisotropic permittivity and permeability [19, ch. 1] are sufficient to characterize the electric and magnetic macroscopic properties of the fundamental Floquet modes of the arrays; that is, the macroscopic magnetoelectric dyadics of a bianisotropic formulation are not required, even though the arrays may be characterized by strong spatial dispersion in the long wavelength limit in the case of bianisotropic inclusion material. The constitutive parameters (permittivity, inverse permeability, and their associated susceptibilities) of this anisotropic representation have the further advantage of satisfying causality (at each fixed $\boldsymbol{\beta}$) and well-defined (though coupled) reciprocity relations and passivity conditions, while maintaining a convenient decomposition into separate electric and magnetic polarizations.

Interestingly, the generalized electric and magnetic polarization densities do not involve generalized multipole moments of higher order than generalized electric quadrupole moments. As both $\boldsymbol{\beta}$ and ω become sufficiently small, the enforced and free-space wavelengths become much larger than the separation distance d between the unit cells of the inclusions and the periodic-array formulation approaches that of an anisotropic continuum fully described by the permittivity and permeability of the fundamental Floquet mode of the array. Moreover, for array inclusions having nonzero electric and/or magnetic dipole moments as $|\boldsymbol{\beta}d|$ and $|k_0 d|$ both become sufficiently small (where $k_0 = \omega\sqrt{\mu_0\epsilon_0} = \omega/c$), the arrays can be represented by an anisotropic dipolar continuum with negligible higher-order multipole densities. In this anisotropic dipolar continuum, the electric and magnetic fields as well as the polarization densities are defined in terms of the same macroscopic averages used for conventional dipolar continua and thus, for example, in the absence of delta-function surface polarizations, the tangential components of the macroscopic E-electric and H-magnetic fields across interfaces (thin transition layers) between free space and the array or between two arrays become approximately continuous as $|\boldsymbol{\beta}d|$ and $|k_0 d|$ both become sufficiently small.

Within the framework of this macroscopic, spatially dispersive anisotropic formulation, it is significant that diamagnetism presents no unusual causality problems, in that the resulting inverse diamagnetic permeability is shown to exhibit a zero time-domain response for time $t < 0$ and to satisfy the Kramers–Kronig dispersion relations at each fixed $\boldsymbol{\beta}$. That is, the theory requires no special considerations or modifications to achieve a causal response [20] for arrays with inclusions that produce macroscopic diamagnetic permeability.

One of the unusual features of this anisotropic formulation is that the passivity conditions for the macroscopic permittivity and permeability dyadics are coupled at the higher values of $\boldsymbol{\beta}$ or ω such that the

imaginary parts of the diagonal elements of either the permittivity or permeability dyadic can be negative as well as positive (or zero) while power dissipation within the inclusions remains greater than or equal to zero. This departure from spatially nondispersive dipolar continuum behavior of the imaginary parts of the constitutive parameters of the fundamental Floquet modes of the arrays is caused by the strong spatial or temporal dispersion at the higher values of $\boldsymbol{\beta}$ or ω.

Although this macroscopic, spatially dispersive anisotropic representation implies that a macroscopic, spatially dispersive bianisotropic representation of metamaterials is not required, a macroscopic bianisotropic formulation [16,18] may for some applications be more suitable and useful, especially for arrays with magnetoelectric coupling in the material of the inclusions. For example, if magnetoelectric coupling at the inclusion level remains significant as the propagation vector $\boldsymbol{\beta}$ and the frequency ω approach zero, the macroscopic permittivity or permeability in the anisotropic formulation (unlike the macroscopic bianisotropic constitutive parameters) can retain a strong dispersion [21].

The development of the anisotropic representation proceeds from Section 1 to Section 2 in which the basic macroscopic equations for the fundamental Floquet modes of 3D periodic arrays are derived from the microscopic equations for the general lossy or lossless polarizable material of the inclusions of the arrays. Sufficient conditions are given for the array to approximate an electromagnetic continuum, and boundary conditions are determined for an electric quadrupolar continuum.

Section 3 develops the anisotropic constitutive relations for the fundamental Floquet modes of 3D arrays and determines expressions for the full permittivity and permeability dyadics in terms of their components transverse to the propagation vector $\boldsymbol{\beta}$.

In Section 4, the reality conditions, reciprocity relations, passivity conditions, and causality relations are determined for the spatially dispersive anisotropic macroscopic permittivity and permeability.

Lastly, in Section 5 we compute the fundamental Floquet-mode macroscopic permittivity and permeability as $\boldsymbol{\beta}$ approaches zero for a 2D array of circular cylinders comprised of material that satisfies a Drude dielectric model. In accordance with the predictions of the theory, the fundamental Floquet-mode macroscopic permittivity and inverse permeability of the 2D array satisfy causality and the coupled passivity conditions, whereas the fundamental Floquet-mode macroscopic permeability does not satisfy causality.

2. Derivation of Maxwellian macroscopic equations for the fundamental Floquet modes on periodic arrays of lossy or lossless polarizable inclusions

We assume that the inclusions (artificial molecules) of a 3D periodic array can support electric current density $\boldsymbol{\mathcal{J}}_\omega(\mathbf{r})$ (with associated charge density $\rho_\omega(\mathbf{r})$), dipolar electric polarization density $\boldsymbol{\mathcal{P}}_\omega(\mathbf{r})$, and dipolar magnetic polarization density (microscopic Amperian magnetization) $\boldsymbol{\mathcal{M}}_\omega(\mathbf{r})$, where the subscripts "$_\omega$" indicate that $e^{-i\omega t}$ time dependence has been suppressed, and the coordinate system in which $\mathbf{r}$ is measured is fixed with respect to the inclusions. The inclusions are assumed to be electrically separated in free space and comprised of lossy or lossless polarizable material. Thus, the array can be described electromagnetically by the following microscopic (inclusion-level) Maxwell differential equations in the space–frequency ($\mathbf{r}$, ω) domain [22, ch. 1]

$$\nabla \times \boldsymbol{\mathcal{E}}_\omega(\mathbf{r}) - i\omega \boldsymbol{\mathcal{B}}_\omega(\mathbf{r}) = 0 \tag{4a}$$

$$\frac{1}{\mu_0}\nabla \times \boldsymbol{\mathcal{B}}_\omega + i\omega\epsilon_0 \boldsymbol{\mathcal{E}}_\omega - \boldsymbol{\mathcal{J}}^p_\omega - \nabla \times \boldsymbol{\mathcal{M}}_\omega = \boldsymbol{\mathcal{J}}_{a\omega} \tag{4b}$$

$$\nabla \cdot \boldsymbol{\mathcal{B}}_\omega(\mathbf{r}) = 0 \tag{4c}$$

$$\epsilon_0 \nabla \cdot \boldsymbol{\mathcal{E}}_\omega(\mathbf{r}) = \rho^p_\omega(\mathbf{r}) + \rho_{a\omega}(\mathbf{r}) \tag{4d}$$

where the equivalent electric current and charge densities are

$$\boldsymbol{\mathcal{J}}^p_\omega = \boldsymbol{\mathcal{J}}_\omega - i\omega \boldsymbol{\mathcal{P}}_\omega \tag{5a}$$

$$\rho^p_\omega = \rho_\omega - \nabla \cdot \boldsymbol{\mathcal{P}}_\omega\,. \tag{5b}$$

The $\boldsymbol{\mathcal{E}}_\omega$ and $\boldsymbol{\mathcal{B}}_\omega$ vectors are taken as the primary electric and magnetic fields, $\boldsymbol{\mathcal{J}}_{a\omega}(\mathbf{r})$ is the applied electric current density, and μ_0 and ϵ_0 are the free-space permeability and permittivity, respectively. Hypothetical induced and applied magnetic current and charge densities have been taken as zero in (4a) and (4c), respectively, to keep the equations as simple as possible while still allowing the applied electric current density to vary arbitrarily. Also, of course, magnetic currents and charges have never been observed experimentally. The induced and applied electric charge densities, ρ^p_ω and $\rho_{a\omega}$, are related to the induced and applied electric current densities, $\boldsymbol{\mathcal{J}}^p_\omega$ and $\boldsymbol{\mathcal{J}}_{a\omega}$, through the continuity equations

$$\nabla \cdot \boldsymbol{\mathcal{J}}^p_\omega(\mathbf{r}) - i\omega\rho^p_\omega(\mathbf{r}) = 0 \tag{6a}$$

$$\nabla \cdot \mathcal{J}_{a\omega}(\mathbf{r}) - i\omega\rho_{a\omega}(\mathbf{r}) = 0\,. \tag{6b}$$

Assume that the applied electric current density has the general plane-wave dependence

$$\mathcal{J}_{a\omega}(\mathbf{r}) = \mathbf{J}_a(\boldsymbol{\beta},\omega)e^{i\,\boldsymbol{\beta}\cdot\mathbf{r}} \tag{7}$$

with the rectangular components of the propagation vector $\boldsymbol{\beta}$ and the angular frequency ω having independent real values ranging from $-\infty$ to $+\infty$. Then, the periodicity of the array requires that the fields and induced source densities satisfy the Floquet modal equations; for example, the electric field can be expressed as

$$\mathcal{E}_\omega(\mathbf{r}) = e^{i\,\boldsymbol{\beta}\cdot\mathbf{r}} \sum_{(l,m,n)=-(\infty,\infty,\infty)}^{+(\infty,\infty,\infty)} \mathbf{E}_{lmn}(\boldsymbol{\beta},\omega)e^{i\mathbf{b}_{lmn}\cdot\mathbf{r}} \tag{8}$$

and similarly for the magnetic field and source densities. For simplicity, we shall assume a cubic array with lattice spacing d such that

$$\mathbf{b}_{lmn} = \frac{2\pi l}{d}\hat{\mathrm{x}} + \frac{2\pi m}{d}\hat{\mathrm{y}} + \frac{2\pi n}{d}\hat{\mathrm{z}} \tag{9}$$

where $(\hat{\mathrm{x}}, \hat{\mathrm{y}}, \hat{\mathrm{z}})$ are the unit vectors in the (x, y, z) principal directions of a 3D cubic array. Since $\mathbf{b}_{000} = 0$, the $(l, m, n) = (0, 0, 0)$ term in (8) with spatial propagation vector $\boldsymbol{\beta}$ is called the fundamental Floquet mode.

The applied plane-wave current spectrum $\mathbf{J}_a(\boldsymbol{\beta}, \omega)$ in (7) for all real $\boldsymbol{\beta}$ can be used to represent an arbitrary localized applied current density $\mathcal{J}^a_\omega(\mathbf{r})$ through the Fourier transform

$$\mathcal{J}^a_\omega(\mathbf{r}) = \int_{-\infty}^{+\infty}\int_{-\infty}^{+\infty}\int_{-\infty}^{+\infty} \mathbf{J}_a(\boldsymbol{\beta},\omega)e^{i\,\boldsymbol{\beta}\cdot\mathbf{r}}d^3\beta \tag{10a}$$

with $\mathbf{J}_a(\boldsymbol{\beta}, \omega)$ given by the inverse Fourier transform

$$\mathbf{J}_a(\boldsymbol{\beta},\omega) = \frac{1}{(2\pi)^3}\int_{-\infty}^{+\infty}\int_{-\infty}^{+\infty}\int_{-\infty}^{+\infty} \mathcal{J}^a_\omega(\mathbf{r})^{-i\boldsymbol{\beta}\cdot\mathbf{r}}d^3r \tag{10b}$$

and similarly for the accompanying spectra of the fields.

For any fixed value of real $\boldsymbol{\beta}$, arrays of lossless inclusions can have homogeneous (source-free: $\mathbf{J}_a = 0$) "eigenmode" (sometimes called "normal-mode") solutions to (4) and (11) at discrete real frequencies $\omega = \omega_{eig}(\boldsymbol{\beta})$. At these discrete frequencies, the inhomogeneous solution for the fields with applied current density in (7) generally diverges (whereas the macroscopic permittivity and permeability defined in Section 3 remain finite and continuous as $\omega \to \omega_{eig}(\boldsymbol{\beta})$). For both theoretical analyses and numerical solvers, the solution to the lossless array can often be investigated more easily near the eigenmodes at real $(\boldsymbol{\beta}, \omega)$ by inserting a small loss into the material of the inclusions to eliminate the singularities from the solution at real $(\boldsymbol{\beta}, \omega)$. Also, the applied fields will diverge if $\omega = \pm|\boldsymbol{\beta}|/\sqrt{\mu_0\epsilon_0}$ and thus these two values of ω should be avoided. (As an aside, we mention that source-free eigenmodes with complex propagation constants can exist even on lossless arrays [23]. These complex waves can, nonetheless, be represented by an integration of the plane-wave spectra over real $\boldsymbol{\beta}$—as can be demonstrated by closing the contours of the real $\boldsymbol{\beta}$ integrations in the complex $\boldsymbol{\beta}$ planes.)

Inserting the electric field from (8), and the similar Floquet modal expressions for the magnetic field and source densities, into the Maxwell equations in (4), then multiplying the resulting equations by $e^{-i\,\boldsymbol{\beta}\cdot\mathbf{r}}$ and integrating over the volume of any one unit cell, we obtain the spectral domain Maxwellian equations for the fundamental Floquet mode of the array

$$i\boldsymbol{\beta}\times\mathbf{E}(\boldsymbol{\beta},\omega) - i\omega\mathbf{B}(\boldsymbol{\beta},\omega) = 0 \tag{11a}$$

$$\frac{1}{\mu_0}i\boldsymbol{\beta}\times\mathbf{B} + i\omega\epsilon_0\mathbf{E} - \mathbf{J}^p - i\boldsymbol{\beta}\times\mathbf{M} = \mathbf{J}_a \tag{11b}$$

in which we have defined $\mathbf{E}(\boldsymbol{\beta}, \omega) \equiv \mathbf{E}_{000}(\boldsymbol{\beta}, \omega)$ and similarly omitted the "$_{000}$" subscripts on the other fundamental Floquet modal spectra. Likewise, the continuity equations in (6) transform to

$$i\boldsymbol{\beta}\cdot\mathbf{J}^p(\boldsymbol{\beta},\omega) - i\omega\rho^p(\boldsymbol{\beta},\omega) = 0 \tag{12a}$$

$$i\boldsymbol{\beta}\cdot\mathbf{J}_a(\boldsymbol{\beta},\omega) - i\omega\rho_a(\boldsymbol{\beta},\omega) = 0 \tag{12b}$$

with $\rho^p = \rho - i\boldsymbol{\beta}\cdot\mathbf{P}$. The form of these spectral Maxwellian equations for the fundamental Floquet mode is identical to the corresponding continuum spectral equations for applied sources with $e^{i(\boldsymbol{\beta}\cdot\mathbf{r}-\omega t)}$ plane-wave dependence. The divergence equations corresponding to (4c) and (4d) need not be included separately in (11) because they can be obtained (for $\boldsymbol{\beta} \neq 0$ or $\omega \neq 0$) by taking the scalar product of $\boldsymbol{\beta}$ with (11a) and (11b) and using the continuity equations in (12).

Multiplying (8) by $e^{-i\,\boldsymbol{\beta}\cdot\mathbf{r}}$ and integrating over the volume V_c of a unit cell, we find that

$$\mathbf{E}(\boldsymbol{\beta},\omega) = \frac{1}{d^3}\int_{V_c}\mathcal{E}_\omega(\mathbf{r})e^{-i\,\boldsymbol{\beta}\cdot\mathbf{r}}d^3r \tag{13}$$

with similar integral expressions holding for the other fundamental Floquet modal spectra. In particular, the fundamental Floquet-mode induced electric current

spectrum can be expressed as

$$\mathbf{J}^p(\boldsymbol{\beta},\omega)=\frac{1}{d^3}\int_{V_c}\boldsymbol{\mathcal{J}}^p_\omega(\mathbf{r})e^{-i\boldsymbol{\beta}\cdot\mathbf{r}}d^3r\,. \tag{14}$$

To decompose $\mathbf{J}^p(\boldsymbol{\beta},\omega)$ into generalized electric and magnetic polarization densities, begin with the microscopic equivalent electric current density $\boldsymbol{\mathcal{J}}^p_\omega(\mathbf{r})$ and the vector-dyadic identity

$$\boldsymbol{\mathcal{J}}^p_\omega=\nabla\cdot\left(\boldsymbol{\mathcal{J}}^p_\omega\mathbf{r}\right)-(\nabla\cdot\boldsymbol{\mathcal{J}}^p_\omega)\mathbf{r}\,. \tag{15}$$

Re-expressing $\boldsymbol{\mathcal{J}}^p_\omega\mathbf{r}$ as

$$\boldsymbol{\mathcal{J}}^p_\omega\mathbf{r}=\frac{1}{2}(\boldsymbol{\mathcal{J}}^p_\omega\mathbf{r}-\mathbf{r}\boldsymbol{\mathcal{J}}^p_\omega)+\frac{1}{2}(\boldsymbol{\mathcal{J}}^p_\omega\mathbf{r}+\mathbf{r}\boldsymbol{\mathcal{J}}^p_\omega) \tag{16a}$$

and using the identity

$$\nabla\cdot(\boldsymbol{\mathcal{J}}^p_\omega\mathbf{r}-\mathbf{r}\boldsymbol{\mathcal{J}}^p_\omega)=\nabla\times(\mathbf{r}\times\boldsymbol{\mathcal{J}}^p_\omega) \tag{16b}$$

allows the electric current in (15) to be rewritten as [9]

$$\boldsymbol{\mathcal{J}}^p_\omega=-i\omega\rho^p_\omega\mathbf{r}+\frac{1}{2}\nabla\cdot(\boldsymbol{\mathcal{J}}^p_\omega\mathbf{r}+\mathbf{r}\boldsymbol{\mathcal{J}}^p_\omega)+\frac{1}{2}\nabla\times(\mathbf{r}\times\boldsymbol{\mathcal{J}}^p_\omega) \tag{17}$$

with the help of the continuity equation in (6a), where, as in (13) and (14)

$$\rho^p_\omega(\mathbf{r})=e^{i\boldsymbol{\beta}\cdot\mathbf{r}}\sum_{(l,m,n)=-(\infty,\infty,\infty)}^{+(\infty,\infty,\infty)}\rho^p_{lmn}(\boldsymbol{\beta},\omega)e^{i\mathbf{b}_{lmn}\cdot\mathbf{r}}\,. \tag{18}$$

Substitution of $\boldsymbol{\mathcal{J}}^p_\omega$ from (17) into (14) gives

$$\mathbf{J}^p(\boldsymbol{\beta},\omega)=-i\omega\mathbf{P}^e_\rho+\frac{\omega}{2}\boldsymbol{\beta}\cdot\overline{\mathbf{Q}}^e+i\boldsymbol{\beta}\times\mathbf{M}^e \tag{19}$$

with the generalized macroscopic electric charge polarization density $\mathbf{P}^e_\rho(\boldsymbol{\beta},\omega)$, electric current magnetic polarization density $\mathbf{M}^e(\boldsymbol{\beta},\omega)$, and dyadic electric quadrupolar polarization density $\overline{\mathbf{Q}}^e(\boldsymbol{\beta},\omega)$ defined as

$$\mathbf{P}^e_\rho(\boldsymbol{\beta},\omega)=\frac{1}{d^3}\int_{V_c}\rho^p_\omega(\mathbf{r})\mathbf{r}_c e^{-i\boldsymbol{\beta}\cdot\mathbf{r}}d^3r \tag{20a}$$

$$\mathbf{M}^e(\boldsymbol{\beta},\omega)=\frac{1}{2d^3}\int_{V_c}\mathbf{r}_c\times\boldsymbol{\mathcal{J}}^p_\omega(\mathbf{r})e^{-i\boldsymbol{\beta}\cdot\mathbf{r}}d^3r \tag{20b}$$

$$\overline{\mathbf{Q}}^e(\boldsymbol{\beta},\omega)=\frac{i}{\omega d^3}\int_{V_c}[\boldsymbol{\mathcal{J}}^p_\omega(\mathbf{r})\mathbf{r}_c+\mathbf{r}_c\boldsymbol{\mathcal{J}}^p_\omega(\mathbf{r})]e^{-i\boldsymbol{\beta}\cdot\mathbf{r}}d^3r \tag{20c}$$

where $\mathbf{r}_c$ is the position vector measured from a fixed point within the unit cell of integration (so that for the same fixed point with respect to each of the unit cells, the polarization densities in (20) are independent of which unit cell is chosen for the integration). It should be noted that this replacement of the factors $\mathbf{r}$ by $\mathbf{r}_c$ in (20) is valid because (17) holds with the factors $\mathbf{r}$ replaced by $\mathbf{r}_c$. *Moreover, it is assumed that the surface S_c of the volume V_c of the unit cell lies in free space, that is, S_c does not intersect the induced sources of the inclusions, so that the volume integral of the first divergence term on the right-hand side of (15), for example, converts to a surface integral over S_c that is zero.* (Thus, the theory is not directly applicable to electrically connected inclusions such as those that form some wire media.) The superscripts "^{e}" in (20) denote generalized polarization densities produced by the induced equivalent electric charge-current. The effective microscopic electric charge-current polarization densities are found from (20) as

$$\boldsymbol{\mathcal{P}}^e_{\rho\omega}(\mathbf{r})=\rho^p_\omega(\mathbf{r})\mathbf{r}_c \tag{21a}$$

$$\boldsymbol{\mathcal{M}}^e_\omega(\mathbf{r})=\frac{1}{2}\mathbf{r}_c\times\boldsymbol{\mathcal{J}}^p_\omega(\mathbf{r}) \tag{21b}$$

$$\overline{\boldsymbol{\mathcal{Q}}}^e_\omega(\mathbf{r})=-\frac{1}{i\omega}[\boldsymbol{\mathcal{J}}^p_\omega(\mathbf{r})\mathbf{r}_c+\mathbf{r}_c\boldsymbol{\mathcal{J}}^p_\omega(\mathbf{r})]\,. \tag{21c}$$

These effective source densities have the same fundamental $e^{i\boldsymbol{\beta}\cdot\mathbf{r}}$ variation as $\rho^p_\omega(\mathbf{r})$ and $\boldsymbol{\mathcal{J}}^p_\omega(\mathbf{r})$. Observe that $\overline{\boldsymbol{\mathcal{Q}}}^e_\omega(\mathbf{r})$ and $\overline{\mathbf{Q}}^e(\boldsymbol{\beta},\omega)$ are symmetric dyadics. Eqs. (20) are generalizations of similar equations in the "scaling homogenization theory" of [9].

With $\mathbf{J}^p$ in (19) inserted into (11b), we can define a total generalized electric polarization density as

$$\mathbf{P}^e(\boldsymbol{\beta},\omega)\equiv\mathbf{P}^e_\rho(\boldsymbol{\beta},\omega)+\frac{i\boldsymbol{\beta}\cdot\overline{\mathbf{Q}}^e(\boldsymbol{\beta},\omega)}{2} \tag{22}$$

as well as a generalized electric displacement vector $\mathbf{D}$ and a magnetic field vector $\mathbf{H}$ as

$$\mathbf{D}(\boldsymbol{\beta},\omega)\equiv\epsilon_0\mathbf{E}(\boldsymbol{\beta},\omega)+\mathbf{P}^e(\boldsymbol{\beta},\omega) \tag{23a}$$

$$\mathbf{H}(\boldsymbol{\beta},\omega)\equiv\mathbf{B}(\boldsymbol{\beta},\omega)/\mu_0-\mathbf{M}^e(\boldsymbol{\beta},\omega)-\mathbf{M}(\boldsymbol{\beta},\omega). \tag{23b}$$

Then the spectral Maxwellian equations in (11) for the fundamental Floquet mode of the array become

$$i\boldsymbol{\beta}\times\mathbf{E}(\boldsymbol{\beta},\omega)-i\omega\mathbf{B}(\boldsymbol{\beta},\omega)=0 \tag{24a}$$

$$i\boldsymbol{\beta}\times\mathbf{H}(\boldsymbol{\beta},\omega)+i\omega\mathbf{D}(\boldsymbol{\beta},\omega)=\mathbf{J}_a(\boldsymbol{\beta},\omega)\,. \tag{24b}$$

To obtain this traditional form of the macroscopic Maxwell's equations in (24) for these "electric current" polarizable inclusions satisfying the microscopic equations in (4) with $(\boldsymbol{\mathcal{E}}_\omega,\boldsymbol{\mathcal{B}}_\omega)$ as the primary fields, we have had to choose $(\mathbf{E},\mathbf{B})$ as the primary macroscopic fields (obtained from the generalized average, as in (13), of the corresponding microscopic fields) and $(\mathbf{D},\mathbf{H})$ as the

secondary fields defined in (23) in terms of the macroscopic primary fields and the macroscopic polarization densities in (20). The fundamental definitions of the generalized macroscopic polarization densities in (20) in terms of integrals over the microscopic sources at a fixed $\boldsymbol{\beta}$ is what ensures the causality of these polarizations and that of their associated constitutive parameters. These causal integral definitions distinguish themselves from the spherical multipole definitions of polarization in terms of external fields (as in the Mie series), which exhibit an inherent noncausality generated by the finite size of the inclusions [20]. Only as the size of the inclusions become infinitesimal do the integral and spherical multipole definitions yield the same macroscopic polarizations.

The total Floquet-mode equivalent electric current

$$\mathbf{J}^{\text{tot}} = -i\omega\mathbf{P}^e_\rho + \omega\boldsymbol{\beta}\cdot\overline{\mathbf{Q}}^e/2 + i\boldsymbol{\beta}\times[\mathbf{M}^e + \mathbf{M}] \tag{25}$$

is equal to the Landau–Lifshitz single-polarization vector $-i\omega\mathbf{P}_L(\boldsymbol{\beta},\ \omega)$ [2, ch. 12], [13] mentioned in Section 1; that is

$$\mathbf{J}^{\text{tot}}(\boldsymbol{\beta},\omega) = -i\omega\mathbf{P}_L(\boldsymbol{\beta},\omega)\,. \tag{26}$$

Eqs. (23) and (24) are noteworthy, not only because they are Maxwellian equations for the fundamental Floquet modes of 3D arrays of lossy or lossless polarizable inclusions, but also because they involve no generalized multipole moments of higher order than the generalized electric quadrupole moment contained in (22) as part of the total generalized electric polarization density $\mathbf{P}^e(\boldsymbol{\beta},\ \omega)$. Moreover, the fields $\mathbf{E}$ and $\mathbf{D}$ involve only electric type quantities and the fields $\mathbf{B}$ and $\mathbf{H}$ involve only magnetic type quantities.

The generalized electric-quadrupole polarization in (22) is grouped with the generalized electric-dipole polarization rather than the generalized magnetic-dipole polarization because an expansion of the generalized electric-dipole polarization in (20a) as $\boldsymbol{\beta}\to 0$ produces a term equal to $-i\boldsymbol{\beta}\cdot\overline{\mathbf{Q}}^e$; see (29). Combining the electric dipole and quadrupole moments into a single electric polarization allows a single bulk permittivity dyadic $\overline{\boldsymbol{\epsilon}}$ in Section 3 to characterize the electric properties of the array. However, this bulk permittivity dyadic does not reveal how much of the macroscopic polarization is contributed individually by the generalized electric-dipole polarization $\mathbf{P}^e_\rho$ and the electric-quadrupole polarization $\overline{\mathbf{Q}}^e$. If desirable, it is a simple matter to separate the contributions from $\mathbf{P}^e_\rho$ and $i\boldsymbol{\beta}\cdot\overline{\mathbf{Q}}^e/2$ to the bulk permittivity dyadic $\overline{\boldsymbol{\epsilon}}$ and thus to determine separate generalized electric-dipole and electric-quadrupole dyadic susceptibilities.

The value of the generalized macroscopic polarizations in (20) and the constitutive parameters (defined in Section 3) depend on the position of the inclusion within the unit cell of integration, or, more precisely, on the position of the origin of the vector $\mathbf{r}_c$ with respect to the inclusion [24]. However, the value of the total macroscopic equivalent electric current $\mathbf{J}^{\text{tot}}(\boldsymbol{\beta},\ \omega)$ in (25), obtained by adding the macroscopic polarizations, is independent of the position of the inclusion within the unit cell, and thus the primary macroscopic fields, $\mathbf{E}(\boldsymbol{\beta},\ \omega)$ and $\mathbf{B}(\boldsymbol{\beta},\ \omega)$ are uniquely defined.

2.1. Definition of an electromagnetic continuum

The foregoing development of the macroscopic equations for the fundamental Floquet modes on 3D arrays provides a convenient set of equations for defining an electromagnetic "continuum." An array of electrically isolated inclusions can be treated as an electromagnetic "continuum" if two conditions are satisfied:

(1) $|\boldsymbol{\beta}d|$ is small enough (generally $|\boldsymbol{\beta}d| \ll 1$)[1] that the ordinary averages (that is, averages without the $e^{-i\,\boldsymbol{\beta}\cdot\mathbf{r}}$ weighting factor) of the microscopic fields and sources over the unit cell approximately equal the fields and sources of the fundamental Floquet mode; for example, for the electric field in (8)

$$\frac{1}{d^3}\int_{\mathrm{V}_c}\boldsymbol{\mathcal{E}}_\omega(\mathbf{r})d^3r = \tag{27}$$

$$\frac{1}{d^3}\int_{\mathrm{V}_c}\Big[e^{i\,\boldsymbol{\beta}\cdot\mathbf{r}}\sum_{(l,m,n)=-(\infty,\infty,\infty)}^{+(\infty,\infty,\infty)}\mathbf{E}_{lmn}e^{i\mathbf{b}_{lmn}\cdot\mathbf{r}}\Big]d^3r \approx \mathbf{E}(\boldsymbol{\beta},\omega)e^{i\,\boldsymbol{\beta}\cdot\mathbf{r}_0}$$

where $\mathbf{r}_0$ is the center of the unit cell, and similarly for the microscopic magnetic field, $\boldsymbol{\mathcal{B}}_\omega(\mathbf{r})$, and the microscopic sources, $\boldsymbol{\mathcal{P}}^e_{\rho\omega}(\mathbf{r})$, $\boldsymbol{\mathcal{M}}^e_\omega(\mathbf{r})$, $\boldsymbol{\mathcal{M}}_\omega(\mathbf{r})$, and $\overline{\boldsymbol{\mathcal{Q}}}^e_\omega(\mathbf{r})$.

(2) $|k_0d| = |\omega d/c|$ is small enough (generally $|k_0d| \ll 1$; see Footnote 1) that the wave numbers $\boldsymbol{\beta}_{\text{eig}}(\omega)$ of the "propagating" source-free eigenmodes of the array

[1] This criterion of "$\ll$1" can sometimes be relaxed to "$<$1" [5], and in the special case of homogeneous inclusion material that occupies nearly the entire volume of the unit cell, the criterion can be relaxed to values greater than 1. Although such a nominally periodic array can be considered a continuum over spatial and frequency bandwidths, $|\boldsymbol{\beta}d|$ and $|k_0d|$, greater than 1, it is a relatively uninteresting case that we shall ignore in the discussion of continua and their boundary conditions in this section and the following Subsection 2.1.1.

(that would be excited by discontinuities or terminations of the array) satisfy the requirement of condition (1) of small enough $|\boldsymbol{\beta}_{\rm eig}d|$ that the fundamental Floquet modes dominate. This second continuum condition implies that the quasi-static fields of the electrically separated inclusions dominate over the length of several or more unit cells. On lossy arrays, the $\boldsymbol{\beta}_{\rm eig}$ of the propagating eigenmodes can be complex with small imaginary parts for small values of $|k_0d|$. In addition, even for small values of $|k_0d|$, there may be "evanescent" complex eigenmodes on lossy and lossless arrays with $|{\rm Im}(\boldsymbol{\beta}_{\rm eig}d)| > 1$ (see, for example, [23, part 2, fig. 10c]). However, these evanescent waves are irrelevant for defining a continuum because they decay to a negligible value in "transition layers" a small fraction of a wavelength from discontinuities or termination surfaces of an array.

If the above conditions (1) and (2) are met, ordinary averages over electrically small (quasi-static) macroscopic volumes ΔV within the array, but outside any transition layers of discontinuities or terminations of the array, and containing many inclusions (such that the surfaces of the macroscopic volumes do not intersect the inclusions) will produce physically meaningful averages at each value of $\boldsymbol{\beta}$ and ω satisfying the small $|\boldsymbol{\beta}d|$ and small $|k_0d|$ criteria of conditions (1) and (2). Specifically,

$$\mathbf{E}_{\rm ave}(\mathbf{r},t) \approx \mathbf{E}(\boldsymbol{\beta},\omega)e^{i(\boldsymbol{\beta}\cdot\mathbf{r}-\omega t)} \tag{28}$$

and similarly for the other fields and source densities. That is, the ordinary macroscopic-volume averages at each $\boldsymbol{\beta}$ and ω within the small spatial and temporal bandwidths defining the continuum are given approximately by the fundamental Floquet mode. The constitutive parameters of a continuum, in particular the permittivity and permeability dyadics defined in Section 3, can be spatially dispersive (as well as temporally dispersive) and even strongly spatially dispersive near inclusion resonances [2, secs. 103–106].

Next, with the help of the polarizations defined in (20), we will show that the continuum can be characterized by ordinary multipole moments with ordinary electric-dipole, magnetic-dipole, and electric-quadrupole moments dominating at sufficiently small values of $|\boldsymbol{\beta}d|$. Consider the integrations in (20) over the unit cell in which the coordinate-system origin of the position vector $\mathbf{r}$ is located, and then let $\mathbf{r}_c = \mathbf{r}$. With $|\boldsymbol{\beta}d|$ sufficiently <1, the approximation $e^{-i\,\boldsymbol{\beta}\cdot\mathbf{r}} \approx 1 - i\boldsymbol{\beta}\cdot\mathbf{r}$ holds for this unit cell and, thus, to first order in $|\boldsymbol{\beta}d|$ (20) yields

$$\mathbf{P}^e_\rho(\boldsymbol{\beta},\omega) = \mathbf{P}^e_0 - i\boldsymbol{\beta}\cdot\overline{\mathbf{Q}}^e_0 + O(|\boldsymbol{\beta}d|^2) \tag{29a}$$

$$\mathbf{M}^e(\boldsymbol{\beta},\omega) + \mathbf{M}(\boldsymbol{\beta},\omega) = \mathbf{M}^e_0 + \mathbf{M}_0 + O(|\boldsymbol{\beta}d|) \tag{29b}$$

where the ordinary (continuum) electric and magnetic dipole-moment densities, and the ordinary electric quadrupole-moment density in the unit cell containing the origin of the position vector $\mathbf{r}$ are given by

$$\mathbf{P}^e_0(\boldsymbol{\beta},\omega) = \frac{1}{d^3}\int_{\rm V_c}[\rho_\omega(\mathbf{r})\mathbf{r} + \boldsymbol{\mathcal{P}}_\omega(\mathbf{r})]d^3r \tag{30a}$$

$$\mathbf{M}^e_0(\boldsymbol{\beta},\omega) = \frac{1}{2d^3}\int_{\rm V_c}\mathbf{r}\times\boldsymbol{\mathcal{J}}^p_\omega(\mathbf{r})d^3r \tag{30b}$$

$$\overline{\mathbf{Q}}^e_0(\boldsymbol{\beta},\omega) = \frac{1}{d^3}\int_{\rm V_c}\rho^p_\omega(\mathbf{r})\mathbf{r}\mathbf{r}d^3r \tag{30c}$$

with the equality in (30a) proven with the help of the identity $\int_{\rm V_c}(\nabla\cdot\boldsymbol{\mathcal{P}}_\omega)\mathbf{r}d^3r = -\int_{\rm V_c}\boldsymbol{\mathcal{P}}_\omega d^3r$, and the equality in (30c) for the ordinary electric quadrupole-moment density proven in several textbooks such as [25, pp. 82–83]. Using the results in (29), the average polarization densities can be expressed in terms of the ordinary average electric, magnetic, and electric quadrupolar moments of the continuum; specifically

$$\mathbf{P}^e_{\rm ave}(\mathbf{r},t) \approx \mathbf{P}^e_{\rm 0ave}(\mathbf{r},t) - \frac{i\boldsymbol{\beta}\cdot\overline{\mathbf{Q}}^e_{\rm 0ave}(\mathbf{r},t)}{2} \tag{31a}$$

$$\mathbf{M}^e_{\rm ave} + \mathbf{M}_{\rm ave} \approx \mathbf{M}^e_{\rm 0ave}(\mathbf{r},t) + \mathbf{M}_{\rm 0ave}(\mathbf{r},t) \tag{31b}$$

Multiplying Eqs. (23) and (24) by $e^{i(\boldsymbol{\beta}\cdot\mathbf{r}-\omega t)}$, then inserting the expressions in (28)–(31) for the fields and polarization densities into these equations, and lastly taking the four-fold $(\boldsymbol{\beta},\omega)$ Fourier transform shows that to first order in $|\boldsymbol{\beta}d|$ the macroscopic fields of the continuum array satisfy the following Maxwell macroscopic space–time continuum equations

$$\nabla\times\boldsymbol{\mathcal{E}}_{\rm ave}(\mathbf{r},t) + \frac{\partial\boldsymbol{\mathcal{B}}_{\rm ave}(\mathbf{r},t)}{\partial t} = 0 \tag{32a}$$

$$\nabla\times\boldsymbol{\mathcal{H}}_{\rm ave}(\mathbf{r},t) - \frac{\partial\boldsymbol{\mathcal{D}}_{\rm ave}(\mathbf{r},t)}{\partial t} = \boldsymbol{\mathcal{J}}^{\rm a}(\mathbf{r},t) \tag{32b}$$

$$\nabla\cdot\boldsymbol{\mathcal{B}}_{\rm ave}(\mathbf{r},t) = 0 \tag{32c}$$

$$\nabla\cdot\boldsymbol{\mathcal{D}}_{\rm ave}(\mathbf{r},t) = \rho^{\rm a}(\mathbf{r},t) \tag{32d}$$

with

$$\boldsymbol{\mathcal{D}}_{\rm ave}(\mathbf{r},t) \approx \epsilon_0\boldsymbol{\mathcal{E}}_{\rm ave} + \boldsymbol{\mathcal{P}}^e_{\rm 0ave} - \frac{1}{2}\nabla\cdot\overline{\boldsymbol{\mathcal{Q}}}^e_{\rm 0ave} \tag{33a}$$

$$\boldsymbol{\mathcal{H}}_{\rm ave}(\mathbf{r},t) \approx \boldsymbol{\mathcal{B}}_{\rm ave}/\mu_0 - \boldsymbol{\mathcal{M}}^e_{\rm 0ave} - \boldsymbol{\mathcal{M}}_{\rm 0ave} \tag{33b}$$

for $\mathcal{J}^{a}(\mathbf{r},t)$ [see (10a)] within the spatial and temporal bandwidths ($\Delta\boldsymbol{\beta}$ and $\Delta\omega$) of the largest sufficiently small $|\boldsymbol{\beta}d|$ and $|k_0 d|$ for the approximations in (27) and (28) to hold and all multipole polarization densities of higher order than $\mathcal{P}^{e}_{0\text{ave}}(\mathbf{r},t)$, $\mathcal{M}^{e}_{0\text{ave}}(\mathbf{r},t)+\mathcal{M}_{0\text{ave}}(\mathbf{r},t)$, and $\overline{\mathcal{Q}}^{e}_{0\text{ave}}(\mathbf{r},t)$ (the ordinary electric-dipole, magnetic-dipole, and electric-quadrupole space–time polarization densities) to be negligible, where from (28) we have

$$\boldsymbol{\mathcal{E}}_{\text{ave}}(\mathbf{r},t)=\int_{-\Delta\omega}^{+\Delta\omega}\int_{-\Delta\boldsymbol{\beta}}^{+\Delta\boldsymbol{\beta}}\mathbf{E}(\boldsymbol{\beta},\omega)e^{i(\boldsymbol{\beta}\cdot\mathbf{r}-\omega t)}d^3\beta d\omega \tag{34}$$

and similarly for the other space–time averages. If the multipole polarization densities of higher order than $\mathcal{P}^{e}_{0\text{ave}}(\mathbf{r},t)$, $\mathcal{M}^{e}_{0\text{ave}}(\mathbf{r},t)+\mathcal{M}_{0\text{ave}}(\mathbf{r},t)$, and $\overline{\mathcal{Q}}^{e}_{0\text{ave}}(\mathbf{r},t)$ are not all negligible over the continuum bandwidths ($\Delta\boldsymbol{\beta}$ and $\Delta\omega$), then the integrals in (20) could be further expanded as in (29) beyond the first-order $|\beta d|$ terms, similarly to what is done in [18], to obtain ordinary multipole densities in (33) of higher order than the dipolar and electric quadrupolar polarization densities. In other words, one retains only the multipole moments of the induced sources that contribute significantly to the E-electric and B-magnetic primary fields within their continuum bandwidths $\Delta\boldsymbol{\beta}$ and $\Delta\omega$. Furthermore, if desirable, the individual contributions from each of these multipole polarizations to the macroscopic permittivity $\overline{\boldsymbol{\epsilon}}(\boldsymbol{\beta},\omega)$ and permeability $\overline{\boldsymbol{\mu}}_{tt}(\boldsymbol{\beta},\omega)$ defined in Section 3 can be used to determine separate multipole susceptibilities for small $|\boldsymbol{\beta}d|$ and all temporal frequencies ω. These multipole susceptibilities at each fixed value of $\boldsymbol{\beta}$, unlike the conventional multipole susceptibilities that are functions of ω only, will be causal functions of ω by the same arguments used in Section 4.4. Fortunately, as explained next, multipole moments higher order than dipolar and sometimes electric quadrupolar are seldom required within the continuum bandwidths.

With the expressions in (29) and (30) substituted into (25), the total current is given to first order in $\boldsymbol{\beta}$ as

$$\mathbf{J}^{\text{tot}}=-i\omega\mathbf{P}^{e}_{0}-\frac{\omega}{2}\boldsymbol{\beta}\cdot\overline{\mathbf{Q}}^{e}_{0}+i\boldsymbol{\beta}\times\left[\mathbf{M}^{e}_{0}+\mathbf{M}_{0}\right]+O(|\boldsymbol{\beta}d|^2). \tag{35}$$

Because the microscopic current and charge densities, $\mathcal{J}^{p}_{\omega}(\mathbf{r})$ and $\rho^{p}_{\omega}(\mathbf{r})$, induced on polarizable or perfectly conducting inclusions are absolutely integrable (so that all the multipole-moment densities are finite), we see from (29a) that for $|\boldsymbol{\beta}d|$ small enough the electric quadrupole-moment density contributes negligibly to the electric polarization and both the electric and magnetic polarizations in (23) become equal to the ordinary electric and magnetic dipole moments per unit-cell volume. Higher order multipole moments do not have to be taken into account in order to determine the macroscopic permittivity for $|\boldsymbol{\beta}d|$ sufficiently small (unless the electric dipole polarization $\mathbf{P}^{e}_{0}(\boldsymbol{\beta},\omega)$ is negligible for $|\boldsymbol{\beta}d|$ less than some finite value).

However, both the electric quadrupole-moment density and magnetic dipole-moment density contribute to order $\boldsymbol{\beta}$ in (35) as $\boldsymbol{\beta}\to 0$ and thus generally both have to be taken into account (at higher temporal frequencies ω) in determining the macroscopic permeability as $\boldsymbol{\beta}\to 0$ [26, p. 61], [24]. However, as $\boldsymbol{\beta}\to 0$, the permeability does not explicitly reveal the contribution to the fields from the electric-quadrupole polarization for an applied magnetic field [21, problem 2, sec. 5.1]. Nonetheless, for $|k_0 d|$ sufficiently small, we see from (35) that the contribution of the electric quadrupole-moment density becomes negligible compared to that of a nonzero magnetic dipole-moment density.

In summary, as both $|\boldsymbol{\beta}d|$ and $|k_0 d|$ become small, the enforced and free-space wavelengths become much larger than the separation distance d between the inclusions, and the anisotropic formulation for the fundamental Floquet mode approaches that of an anisotropic continuum with ordinary electric-dipole, magnetic-dipole, and electric quadrupole polarization densities. *In addition, we have shown that a metamaterial array with inclusions having nonzero electric and/or magnetic dipole moments at low spatial and temporal frequencies (that is, for $|\boldsymbol{\beta}d|$ and $|k_0 d|$ sufficiently small) can be represented by an anisotropic dipolar continuum with negligible higher-order multipole-moment densities.* Since most molecules can be modeled by polarizable or perfectly conducting inclusions, this result also holds for most natural materials with electrically isolated molecules at sufficiently low spatial and temporal frequencies [27, p. 111]. The fields of the dipolar continuum satisfy the space–time Maxwellian equations in (32) and (33) with the electric quadrupole density $\overline{\mathcal{Q}}^{e}_{0\text{ave}}(\mathbf{r},t)=0$.

Before leaving this section, we note that the continuum criterion for the average fields of the array to be well approximated by the fundamental Floquet mode does not imply that the power flow in the higher-order modes of the array continuum must be negligible compared to the power flow in the fundamental Floquet mode (especially if there is strong spatial dispersion) [28,29].

2.1.1. Boundary conditions for electric quadrupolar continua

The Maxwellian macroscopic space–time continuum equations in (32) and (33) hold for applied current excitations with spatial and temporal bandwidths ($\Delta\boldsymbol{\beta}$ and $\Delta\omega$) determined by small enough $|\boldsymbol{\beta}d|$ and $|k_0 d|$, respectively, for the approximations in (27)–(31) to be sufficiently accurate that ordinary macroscopic averaging applies over macroscopic volumes ΔV containing many inclusions. These Eqs. (32) and (33) were derived for infinite periodic arrays of separated inclusions with small enough $|\boldsymbol{\beta}d|$ and $|k_0 d|$ that all multipole-moment polarization densities of higher order than ordinary dipolar and electric quadrupolar polarization densities are negligible. In this subsection, we want to terminate the infinite array in a surface S that is effectively planar in the sense that any subsurface S_p of S extending a distance less than several lattice distances d is approximately planar. The surface S is assumed to be an interface between the array and free space or another array and we want to determine the boundary conditions across this interface.

The termination of the array(s) by the surface S introduces strong spatial variations of the fields and induced sources in the vicinity of S that invalidates the approximations in (27) and (28). Although averages of the microscopic fields and induced sources can still be performed using macroscopic volumes ΔV throughout all space, the resulting macroscopic fields will not generally satisfy (32) and (33) in a transition layer [30, p. 271] containing the interface surface S. For the original infinite continuum arrays characterized by $|\Delta\boldsymbol{\beta}d| \ll 1$ and $|\Delta k_0 d| = \Delta\omega d/c \ll 1$, the thickness δ of the transition layer is much smaller than the free-space and $2\pi/|\boldsymbol{\beta}|$ wavelengths; see discussion of evanescent eigenmodes in the previous section. The effect of this transition layer can be represented in Eqs. (32) by additional transition-layer electric and magnetic current and charge densities on the right-hand sides of the equations in (32). For example, (32a) and (32b) become

$$\nabla \times \boldsymbol{\mathcal{E}}_{\text{ave}}(\mathbf{r},t) + \frac{\partial \boldsymbol{\mathcal{B}}_{\text{ave}}(\mathbf{r},t)}{\partial t} = -\boldsymbol{\mathcal{K}}_{\delta}(\mathbf{r},t) \tag{36a}$$

$$\nabla \times \boldsymbol{\mathcal{H}}_{\text{ave}}(\mathbf{r},t) - \frac{\partial \boldsymbol{\mathcal{D}}_{\text{ave}}(\mathbf{r},t)}{\partial t} = \boldsymbol{\mathcal{J}}^{\text{a}}(\mathbf{r},t) + \boldsymbol{\mathcal{J}}_{\delta}(\mathbf{r},t) \tag{36b}$$

where $\boldsymbol{\mathcal{J}}_{\delta}(\mathbf{r},t)$ and $\boldsymbol{\mathcal{K}}_{\delta}(\mathbf{r},t)$ are transition-layer macroscopic electric and magnetic current densities, respectively, that are zero everywhere except within the transition layer of thickness δ. These equations in (36), along with the constitutive equations in (33), now hold throughout all space. The two divergence equations associated with (36) can be obtained by taking the divergence of the equations in (36). Note from (33a) that $\boldsymbol{\mathcal{P}}^{e}_{\text{ave}}(\mathbf{r},t)$ effectively contains a delta function across the thin transition layer if the electric quadrupole density is not negligible and differs in value on either side of the transition layer; specifically

$$\begin{aligned}\boldsymbol{\mathcal{P}}^{e}_{\text{ave}}(\mathbf{r},t) &= \boldsymbol{\mathcal{P}}^{e}_{0\text{ave}}(\mathbf{r},t) - \frac{1}{2}\nabla\cdot\overline{\boldsymbol{\mathcal{Q}}}^{e}_{0\text{ave}}(\mathbf{r},t)\\ &= \boldsymbol{\mathcal{P}}^{e}_{0\text{ave}}(\mathbf{r},t) - \frac{1}{2}[\nabla\cdot\overline{\boldsymbol{\mathcal{Q}}}^{e}_{0\text{ave}}(\mathbf{r},t)]_{\text{dfr}}\\ &\quad -\frac{1}{2}\hat{\mathrm{n}}\cdot(\overline{\boldsymbol{\mathcal{Q}}}^{e2}_{0\text{ave}} - \overline{\boldsymbol{\mathcal{Q}}}^{e1}_{0\text{ave}})\delta(n)\end{aligned} \tag{37}$$

in which $\hat{\mathrm{n}}$ is the unit normal to the surface S pointing from the side "1" to side "2" of the transition layer, and $\delta(n)$ is the delta function in the normal coordinate n. The subscript "$_{\text{dfr}}$" means "delta function removed" from the divergence of the electric quadrupole dyadic, so that $[\nabla\cdot\overline{\boldsymbol{\mathcal{Q}}}^{e}_{0\text{ave}}(\mathbf{r},t)]_{\text{dfr}}$ can be discontinuous but otherwise nonsingular across the thin transition layer. We are assuming that there are no effective delta functions in the macroscopic dipolar and electric quadrupolar polarization densities, $\boldsymbol{\mathcal{P}}^{e}_{0\text{ave}}(\mathbf{r},t)$, $\boldsymbol{\mathcal{M}}^{e}_{0\text{ave}}(\mathbf{r},t) + \boldsymbol{\mathcal{M}}_{0\text{ave}}(\mathbf{r},t)$, and $\overline{\boldsymbol{\mathcal{Q}}}^{e}_{0\text{ave}}(\mathbf{r},t)$, represented by $\boldsymbol{\mathcal{J}}_{\delta}(\mathbf{r},t)$ and $\boldsymbol{\mathcal{K}}_{\delta}(\mathbf{r},t)$ within the thin transition layer.[2]

Boundary conditions on the tangential components of the macroscopic $\boldsymbol{\mathcal{E}}_{\text{ave}}$ and $\boldsymbol{\mathcal{H}}_{\text{ave}}$ fields and on the normal components of the macroscopic $\boldsymbol{\mathcal{D}}_{\text{ave}}$ and $\boldsymbol{\mathcal{B}}_{\text{ave}}$ fields across the transition layer can be determined by applying the integral forms of (36) and the corresponding divergence equations to thin rectangular closed curves and closed surfaces (pillboxes) with their long dimensions of length ℓ on either side of the transition layer so that their short sides are of width $\delta \ll \ell$ (taking into account the effective delta functions in $\nabla\cdot\overline{\boldsymbol{\mathcal{Q}}}^{e}_{0\text{ave}}$ across the transition layer). Although $\ell \gg \delta$, it is assumed that ℓ is short enough that the macroscopic fields and sources along the length of ℓ do

[2] Delta functions $\delta(n)$ and their derivatives in the polarizations as represented by $\boldsymbol{\mathcal{J}}_{\delta}(\mathbf{r},t)$ and $\boldsymbol{\mathcal{K}}_{\delta}(\mathbf{r},t)$ may exist if these polarizations are proportional to unusually high spatial derivatives of the fields, that is, if they display strong enough spatial dispersion. In that case, the boundary conditions in (38) may have to be modified. However, significant polarization proportional to unusually high spatial derivatives of the fields generally indicates the presence of higher-order multipoles. For example, $\boldsymbol{\mathcal{P}}^{e}_{0\text{ave}}$ proportional to the second spatial derivative of $\boldsymbol{\mathcal{E}}_{\text{ave}}$ would indicate the presence of magnetic dipoles or electric quadrupoles. Similarly, $\boldsymbol{\mathcal{M}}^{e}_{0\text{ave}}$ or $\overline{\boldsymbol{\mathcal{Q}}}^{e}_{0\text{ave}}$ proportional to the second or third spatial derivatives of $\boldsymbol{\mathcal{B}}_{\text{ave}}$ or $\boldsymbol{\mathcal{E}}_{\text{ave}}$, respectively, would indicate the presence of octopoles.

not change appreciably. This determination of boundary conditions for the equations in (36) with the constitutive relations in (33) and (37) has been done in [31] but without the transition current densities, $\mathcal{J}_\delta(\mathbf{r},t)$ and $\mathcal{K}_\delta(\mathbf{r},t)$. However, the additional integrals over $\mathcal{J}_\delta(\mathbf{r},t)$ and $\mathcal{K}_\delta(\mathbf{r},t)$ become insignificant for δ sufficiently small, or equivalently, for $|\Delta\boldsymbol{\beta}d|$ and $|\Delta k_0 d|$ sufficiently small, provided, as discussed in Footnote (2), that $\mathcal{J}_\delta(\mathbf{r},t)$ and $\mathcal{K}_\delta(\mathbf{r},t)$ do not contain delta functions. Thus, we can apply the boundary conditions derived in [31][3] with the surface polarization $\mathbf{P}^\delta$ in [31] replaced by $-\hat{\mathrm{n}}\cdot(\overline{\boldsymbol{Q}}^{e2}_{0\mathrm{ave}}-\overline{\boldsymbol{Q}}^{e1}_{0\mathrm{ave}})/2$ given in (37), to get

$$\boldsymbol{\mathcal{E}}^{2s}_{\mathrm{ave}}-\boldsymbol{\mathcal{E}}^{1s}_{\mathrm{ave}}\approx\frac{1}{2\epsilon_0}\nabla_s\left[\hat{\mathrm{n}}\cdot(\overline{\boldsymbol{Q}}^{e2}_{0\mathrm{ave}}-\overline{\boldsymbol{Q}}^{e1}_{0\mathrm{ave}})\cdot\hat{\mathrm{n}}\right] \tag{38a}$$

$$\boldsymbol{\mathcal{H}}^{2s}_{\mathrm{ave}}-\boldsymbol{\mathcal{H}}^{1s}_{\mathrm{ave}}\approx\frac{1}{2}\hat{\mathrm{n}}\times\frac{\partial}{\partial t}\left[(\hat{\mathrm{n}}\cdot\overline{\boldsymbol{Q}}^{e2}_{0\mathrm{ave}})^{s}-(\hat{\mathrm{n}}\cdot\overline{\boldsymbol{Q}}^{e1}_{0\mathrm{ave}})^{s}\right] \tag{38b}$$

$$\boldsymbol{\mathcal{D}}^{2n}_{\mathrm{ave}}-\boldsymbol{\mathcal{D}}^{1n}_{\mathrm{ave}}\approx\frac{1}{2}\nabla_s\cdot\left[(\hat{\mathrm{n}}\cdot\overline{\boldsymbol{Q}}^{e2}_{0\mathrm{ave}})^{s}-(\hat{\mathrm{n}}\cdot\overline{\boldsymbol{Q}}^{e1}_{0\mathrm{ave}})^{s}\right] \tag{38c}$$

$$\boldsymbol{\mathcal{B}}^{2n}_{\mathrm{ave}}-\boldsymbol{\mathcal{B}}^{1n}_{\mathrm{ave}}\approx 0 \tag{38d}$$

where the superscripts "s" and "n" refer to vector components tangential and normal to the surface S, respectively, and we note that $\overline{\boldsymbol{Q}}^{e}_{0\mathrm{ave}}(\mathbf{r},t)$ is a symmetric dyadic because $\overline{\mathbf{Q}}^{e}_{0}(\boldsymbol{\beta},\omega)$ is a symmetric dyadic. These boundary conditions show that the change in electric quadrupole density across the thin transition layer produces discontinuities in the tangential components of $\boldsymbol{\mathcal{E}}_{\mathrm{ave}}$ and $\boldsymbol{\mathcal{H}}_{\mathrm{ave}}$ and in the normal component of $\boldsymbol{\mathcal{D}}_{\mathrm{ave}}$. They agree with the boundary conditions of Raab and De Lange [24, eqs. (6.69)–(6.74)] if a term $\epsilon_0^{-1}\partial Q_{zz}/\partial z/2$ is added to the right-hand side of [24, eq. (6.71)]. In a private communication, Raab and De Lange have confirmed the necessity of this added term. Our expressions in (38) have also been confirmed in an unpublished independent derivation by M.G. Silveirinha using transverse averaging and assuming no delta-function contributions, as discussed in Footnote (2), from the effective polarizations in the transition layer [32]. In [31] we also prove that $\boldsymbol{\mathcal{E}}^{n}_{\mathrm{ave}}$ has a delta function in the transition layer equal to $\hat{n}\cdot(\overline{\boldsymbol{Q}}^{2}_{0\mathrm{ave}}-\overline{\boldsymbol{Q}}^{1}_{0\mathrm{ave}})\cdot\hat{n}\delta(n)/(2\epsilon_0)$.

[3] The field symbols on the left-hand sides of Eqs. (13), (15), and (16) in [31] should be boldface, and the ∇ symbol one line below Eq. (12) of [31] should be ∇_s.

The results of several analyses and simulations of periodic arrays, for example those in [32–34], indicate that the effect of the boundary layer becomes negligible for spatial and temporal bandwidths, $|\Delta\boldsymbol{\beta}d|$ and $|\Delta k_0 d|$, less than about 0.1. Thus, one would also expect that the boundary conditions in (38) are reliable approximations for $|\Delta\boldsymbol{\beta}d|$ and $|\Delta k_0 d|$ less than about 0.1. If, as discussed in the previous section, these spatial and temporal bandwidths are small enough for the electric quadrupole density to be negligible compared to the dipolar polarization densities, then the electric quadrupole terms in (38) can be neglected and (38) predicts the usual continuity of the tangential $\boldsymbol{\mathcal{E}}_{\mathrm{ave}}$ and $\boldsymbol{\mathcal{H}}_{\mathrm{ave}}$ fields and the normal $\boldsymbol{\mathcal{D}}_{\mathrm{ave}}$ field (as well as the normal $\boldsymbol{\mathcal{B}}_{\mathrm{ave}}$ field) across the thin transition layer. Lastly, we mention the need for more analysis and simulations to investigate the possibility of additional delta functions, as discussed in Footnote (2), in the polarizations of more strongly spatially dispersive arrays and to determine additional boundary conditions (ABCs) for these arrays [8,13].

3. Anisotropic constitutive relations

To formulate an anisotropic description of the fundamental Floquet modes on 3D periodic arrays, we note that for linear inclusion material all the field vectors in (24) are linearly related to the applied electric current vector $\mathbf{J}_{\mathrm{a}}$ and thus we can express $\mathbf{D}$ in terms of $\mathbf{E}$ as

$$\mathbf{D}(\boldsymbol{\beta},\omega)=\overline{\boldsymbol{\epsilon}}_e(\boldsymbol{\beta},\omega)\cdot\mathbf{E}(\boldsymbol{\beta},\omega) \tag{39}$$

with the permittivity dyadic $\overline{\boldsymbol{\epsilon}}_e(\boldsymbol{\beta},\omega)$.

It is somewhat more involved to obtain a viable constitutive relation between the secondary magnetic field $\mathbf{H}$ and the primary magnetic field $\mathbf{B}$ because (24a) shows that the longitudinal (parallel to the propagation vector $\boldsymbol{\beta}$) component of $\mathbf{B}$ is zero ($\boldsymbol{\beta}\cdot\mathbf{B}=0$); that is, denoting longitudinal components by the subscript "$_{\mathrm{l}}$", we have $\mathbf{B}_{\mathrm{l}}=\mu_0(\mathbf{H}_{\mathrm{l}}+\mathbf{M}^{e}_{\mathrm{l}}+\mathbf{M}_{\mathrm{l}})=0$, and $\mathbf{H}$ cannot be expressed in terms of only the two independent components of $\mathbf{B}=\mathbf{B}_{\mathrm{t}}$ where the subscript "$_{\mathrm{t}}$" denotes components transverse to the propagation vector $\boldsymbol{\beta}$. Nonetheless, it is permissible to linearly relate $\mathbf{H}$ to any three independent components of the primary fields. In particular, choosing ($\mathbf{B}$, $\mathbf{E}_{\mathrm{l}}$) as these three primary components, the $\mathbf{H}=\mathbf{H}_{\mathrm{t}}+\mathbf{H}_{\mathrm{l}}$ field can be expressed as

$$\mathbf{H}_{\mathrm{l}}(\boldsymbol{\beta},\omega)=-\mathbf{M}^{e}_{\mathrm{l}}(\boldsymbol{\beta},\omega)-\mathbf{M}_{\mathrm{l}}(\boldsymbol{\beta},\omega) \tag{40}$$

$$\mathbf{H}_{\mathrm{t}}(\boldsymbol{\beta},\omega)=\overline{\boldsymbol{\mu}}^{-1}_{tt}(\boldsymbol{\beta},\omega)\cdot\mathbf{B}(\boldsymbol{\beta},\omega)+\overline{\mathbf{v}}_{tl}(\boldsymbol{\beta},\omega)\cdot\mathbf{E}_{\mathrm{l}}(\boldsymbol{\beta},\omega) \tag{41}$$

where $\overline{\boldsymbol{\mu}}_{tt}(\boldsymbol{\beta},\omega)$ is a transverse permeability dyadic and $\overline{\boldsymbol{\nu}}_{tl}(\boldsymbol{\beta},\omega)$ is a magnetoelectric dyadic. In a rectangular (x, y, z) coordinate system with $\boldsymbol{\beta}$ aligned with one of the axes, $\overline{\boldsymbol{\mu}}_{tt}(\boldsymbol{\beta},\omega)$ and its inverse $\overline{\boldsymbol{\mu}}_{tt}^{-1}(\boldsymbol{\beta},\omega)$ are 2×2 dyadics and $\overline{\boldsymbol{\nu}}_{tl}(\boldsymbol{\beta},\omega)$ is a 2×1 dyadic. (For $\boldsymbol{\beta}$ in directions other than either the x, y, or z direction, the dyadic $\overline{\boldsymbol{\mu}}_{tt}(\boldsymbol{\beta},\omega)$ has nine elements but only four are independent because $\boldsymbol{\beta}\cdot\overline{\boldsymbol{\mu}}_{tt}(\boldsymbol{\beta},\omega)=\overline{\boldsymbol{\mu}}_{tt}(\boldsymbol{\beta},\omega)\cdot\boldsymbol{\beta}=0$, which gives six homogeneous equations from which five of the elements can be written in terms of the other four elements.) The magnetic constitutive parameters $(\overline{\boldsymbol{\mu}}_{tt}^{-1},\overline{\boldsymbol{\nu}}_{tl})$ have a total of six independent elements, the same number of independent elements as a 2×3 permeability dyadic. In (42)–(44a), the magnetoelectric dyadic in (41) is assimilated into the permittivity dyadic to maintain a purely anisotropic (as opposed to bianisotropic) representation of the array.

With the constitutive relations inserted from (39) and (41) into (24), the fundamental Floquet-mode equations in (24) can be recast in the form of the traditional Maxwellian macroscopic equations in an anisotropic medium with primary fields $\mathbf{E}$ and $\mathbf{B}$, namely

$$i\boldsymbol{\beta}\times\mathbf{E}(\boldsymbol{\beta},\omega)-i\omega\mathbf{B}(\boldsymbol{\beta},\omega)=0 \tag{42a}$$

$$i\boldsymbol{\beta}\times\overline{\boldsymbol{\mu}}_{tt}^{-1}\cdot\mathbf{B}+i\omega\overline{\boldsymbol{\epsilon}}\cdot\mathbf{E}=\mathbf{J}_{\mathsf{a}} \tag{42b}$$

where

$$\overline{\boldsymbol{\epsilon}}\equiv\overline{\boldsymbol{\epsilon}}_e+\frac{\boldsymbol{\beta}\times\overline{\boldsymbol{\nu}}_{tl}}{\omega} \tag{43}$$

defines an effective displacement vector

$$\begin{aligned}\mathbf{D}^{\mathrm{eff}}&=\overline{\boldsymbol{\epsilon}}\cdot\mathbf{E}=\epsilon_0\mathbf{E}+\mathbf{P}^e+\boldsymbol{\beta}\times\frac{\overline{\boldsymbol{\nu}}_{tl}\cdot\mathbf{E}_{\mathsf{l}}}{\omega}\\&=\mathbf{D}+\boldsymbol{\beta}\times\frac{\overline{\boldsymbol{\nu}}_{tl}\cdot\mathbf{E}}{\omega}\end{aligned} \tag{44a}$$

and we can define and effective transverse H-field as

$$\begin{aligned}\mathbf{H}_{\mathsf{t}}^{\mathrm{eff}}&=\overline{\boldsymbol{\mu}}_{tt}^{-1}\cdot\mathbf{B}=\frac{\mathbf{B}}{\mu_0}-\mathbf{M}_{\mathsf{t}}^e-\mathbf{M}_{\mathsf{t}}-\overline{\boldsymbol{\nu}}_{tl}\cdot\mathbf{E}_{\mathsf{l}}\\&=\mathbf{H}_{\mathsf{t}}-\overline{\boldsymbol{\nu}}_{tl}\cdot\mathbf{E}_{\mathsf{l}}\end{aligned} \tag{44b}$$

with $\mathbf{H}^{\mathrm{eff}}=\mathbf{H}_{\mathsf{t}}^{\mathrm{eff}}-\mathbf{M}_{\mathsf{l}}^e-\mathbf{M}_{\mathsf{l}}$. Note that, as $\boldsymbol{\beta}/\omega\to 0$, the values of the effective displacement vector $\mathbf{D}^{\mathrm{eff}}$ and permittivity dyadic $\overline{\boldsymbol{\epsilon}}$ become equal to their traditional values (that is, $\mathbf{D}^{\mathrm{eff}}=\mathbf{D}$ and $\overline{\boldsymbol{\epsilon}}=\overline{\boldsymbol{\epsilon}}_e$). Also, for nonbianisotropic inclusions, $\overline{\boldsymbol{\nu}}_{tl}$ becomes negligible at low spatial or temporal frequencies (approaching zero as $\boldsymbol{\beta}\to 0$ or $\omega\to 0$ [21]) and $\mathbf{H}^{\mathrm{eff}}=\mathbf{H}$.

As $\boldsymbol{\beta}\to 0$, it is emphasized that the elements of a transverse dyadic, in particular, the transverse permeability dyadic $\overline{\boldsymbol{\mu}}_{tt}$ (or $\overline{\boldsymbol{\mu}}_{tt}^{-1}$), in an ($x$, y, z) coordinate system fixed in the array, unlike the elements of a complete dyadic such as the permittivity dyadic $\overline{\boldsymbol{\epsilon}}$ (or $\overline{\boldsymbol{\epsilon}}_e$) as $\boldsymbol{\beta}\to 0$, are functions of the direction of $\boldsymbol{\beta}$. Nonetheless, as we explain next, for $\boldsymbol{\beta}\to 0$ the transverse dyadic $\overline{\boldsymbol{\mu}}_{tt}$ can be used to determine a complete permeability dyadic $\overline{\boldsymbol{\mu}}_{\mathsf{b}}$ that relates a $\mathbf{B}_{\mathsf{b}}$ field with three linearly independent components to a corresponding $\mathbf{H}_{\mathsf{b}}$ field.

Consider for the moment the array excited by both applied plane-wave magnetic and electric current densities such that three linearly independent components of the primary fields $\mathbf{E}_{\mathsf{b}}$ and $\mathbf{B}_{\mathsf{b}}$ are generated. The three components of $\mathbf{H}_{\mathsf{b}}$ can be bianisotropically related to the three components of the $\mathbf{E}_{\mathsf{b}}$ and $\mathbf{B}_{\mathsf{b}}$ fields by a complete permeability dyadic $\overline{\boldsymbol{\mu}}_{\mathsf{b}}^{-1}$ and a complete magnetoelectric dyadic $\overline{\boldsymbol{\nu}}_{\mathsf{b}}$; that is

$$\begin{aligned}\mathbf{H}_{\mathsf{b}}(\boldsymbol{\beta},\omega)=\overline{\boldsymbol{\mu}}_{\mathsf{b}}^{-1}(\boldsymbol{\beta},\omega)\cdot\mathbf{B}_{\mathsf{b}}(\boldsymbol{\beta},\omega)+\overline{\boldsymbol{\nu}}_{\mathsf{b}}(\boldsymbol{\beta},\omega)\\\cdot\mathbf{E}_{\mathsf{b}}(\boldsymbol{\beta},\omega).\end{aligned} \tag{45}$$

The nine-element permeability dyadic $\overline{\boldsymbol{\mu}}_{\mathsf{b}}$ can be written in an (x, y, z) coordinate system fixed in the 3D periodic array as

$$\overline{\boldsymbol{\mu}}_{\mathsf{b}}=\begin{bmatrix}\mu_{\mathsf{b}xx}&\mu_{\mathsf{b}xy}&\mu_{\mathsf{b}xz}\\\mu_{\mathsf{b}yx}&\mu_{\mathsf{b}yy}&\mu_{\mathsf{b}yz}\\\mu_{\mathsf{b}zx}&\mu_{\mathsf{b}zy}&\mu_{\mathsf{b}zz}\end{bmatrix}. \tag{46}$$

Setting the applied magnetic current equal to zero, leaving just the applied electric current $\mathbf{J}_{\mathsf{a}}e^{i\,\boldsymbol{\beta}\cdot\mathbf{r}}$, we have $\mathbf{E}_{\mathsf{b}}=\mathbf{E}$, $\mathbf{B}_{\mathsf{b}}=\mathbf{B}=\mathbf{B}_{\mathsf{t}}$ and $\mathbf{H}_{\mathsf{b}}=\mathbf{H}$ so that the transverse part of (45) becomes

$$\mathbf{H}_{\mathsf{t}}=\overline{\boldsymbol{\mu}}_{\mathsf{b}tt}^{-1}\cdot\mathbf{B}+(\overline{\boldsymbol{\nu}}_{\mathsf{b}}\cdot\mathbf{E})_{\mathsf{t}} \tag{47a}$$

or because $\mathbf{E}_{\mathsf{t}}=-\omega\boldsymbol{\beta}\times\mathbf{B}/|\boldsymbol{\beta}|^2=-\omega\overline{\boldsymbol{\beta}}\cdot\mathbf{B}/|\boldsymbol{\beta}|^2$, where $\boldsymbol{\beta}$ is the antisymmetric dyadic corresponding to $\boldsymbol{\beta}\times$

$$\mathbf{H}_{\mathsf{t}}=\left[\overline{\boldsymbol{\mu}}_{\mathsf{b}tt}^{-1}-\omega\overline{\boldsymbol{\nu}}_{\mathsf{b}tt}\cdot\overline{\boldsymbol{\beta}}/|\boldsymbol{\beta}|^2\right]\cdot\mathbf{B}+\overline{\boldsymbol{\nu}}_{\mathsf{b}tl}\cdot\mathbf{E}_{\mathsf{l}}\,. \tag{47b}$$

Comparing (47b) with (41), we see that

$$\overline{\boldsymbol{\mu}}_{\mathsf{b}tt}^{-1}-\omega\overline{\boldsymbol{\nu}}_{\mathsf{b}tt}\cdot\overline{\boldsymbol{\beta}}/|\boldsymbol{\beta}|^2=\overline{\boldsymbol{\mu}}_{tt}^{-1} \tag{48a}$$

$$\overline{\boldsymbol{\nu}}_{\mathsf{b}tl}=\overline{\boldsymbol{\nu}}_{tl}\,. \tag{48b}$$

The bianisotropic term $\omega\overline{\boldsymbol{\nu}}_{\mathsf{b}tt}/|\boldsymbol{\beta}|$ in (48a) is negligible at the lower frequencies ω as $\boldsymbol{\beta}/\omega\to 0$ if the inclusion material does not exhibit bianisotropy [21]. At higher frequencies ω, the lattice bianisotropy, which is $O(\boldsymbol{\beta})$ as $\boldsymbol{\beta}\to 0$ can give a finite value to $\omega\overline{\boldsymbol{\nu}}_{\mathsf{b}tt}/|\boldsymbol{\beta}|$ as $\boldsymbol{\beta}\to 0$ [21]. This finite value can be incorporated into $\overline{\boldsymbol{\mu}}_{\mathsf{b}tt}(\boldsymbol{\beta}\to 0,w)$ in (48a) and is of little consequence because it approaches zero at the lower frequencies ω where the array behaves as a continuum. Thus, for

nonbianisotropic inclusions at low values of ω and $\boldsymbol{\beta} \to 0$, (48a) reduces to

$$\overline{\boldsymbol{\mu}}_{btt}^{-1}(\boldsymbol{\beta} \to 0, \omega) = \overline{\boldsymbol{\mu}}_{tt}^{-1}(\boldsymbol{\beta} \to 0, \omega) \tag{49a}$$

or

$$\overline{\boldsymbol{\mu}}_{btt}(\boldsymbol{\beta} \to 0, \omega) = \overline{\boldsymbol{\mu}}_{tt}(\boldsymbol{\beta} \to 0, \omega)\,. \tag{49b}$$

If we choose the propagation vector $\boldsymbol{\beta}$ in the $\hat{\mathbf{z}}$ direction, the transverse permeability dyadic $\overline{\boldsymbol{\mu}}_{tt}$ can be written as a 2×2 matrix

$$\overline{\boldsymbol{\mu}}_{tt}(\beta_z, \omega) = \begin{bmatrix} \mu_{xx}(\beta_z, \omega) & \mu_{xy}(\beta_z, \omega) \\ \mu_{yx}(\beta_z, \omega) & \mu_{yy}(\beta_z, \omega) \end{bmatrix} \tag{50}$$

and similarly for the $\hat{\mathbf{x}}$ and $\hat{\mathbf{y}}$ directions. Thus, in view of (49), we have

$$\mu_{bxx}(0, \omega) = \mu_{xx}(\beta_z, \omega) = \mu_{xx}(\beta_y, \omega)$$
$$\mu_{bxy}(0, \omega) = \mu_{xy}(\beta_z, \omega) \tag{51a}$$

$$\mu_{byy}(0, \omega) = \mu_{yy}(\beta_z, \omega) = \mu_{yy}(\beta_x, \omega)$$
$$\mu_{byx}(0, \omega) = \mu_{yx}(\beta_z, \omega) \tag{51b}$$

$$\mu_{byz}(0, \omega) = \mu_{yz}(\beta_x, \omega), \quad \mu_{bzy}(0, \omega) = \mu_{zy}(\beta_x, \omega) \tag{51c}$$

$$\mu_{bzz}(0, \omega) = \mu_{zz}(\beta_x, \omega) = \mu_{zz}(\beta_y, \omega) \tag{51d}$$

$$\mu_{bzx}(0, \omega) = \mu_{zx}(\beta_y, \omega), \quad \mu_{bxz}(0, \omega) = \mu_{xz}(\beta_y, \omega) \tag{51e}$$

in which $\beta_x \to 0$, $\beta_y \to 0$, and $\beta_z \to 0$. The results in (51) reveal that, for nonbianisotropic inclusions at low values of ω, the complete permeability dyadic $\overline{\boldsymbol{\mu}}_b(0, \omega)$ of the array, which is independent of the propagation vector $\boldsymbol{\beta}$ (that is, the nine elements of $\overline{\boldsymbol{\mu}}_b(0, \omega)$ do not change with the direction of $\boldsymbol{\beta}$ in an (x, y, z) coordinate system fixed in the array), can be expressed in terms of the transverse propagation-direction dependent permeability dyadic $\overline{\boldsymbol{\mu}}_{tt}(\boldsymbol{\beta} \to 0, \omega)$ in three orthogonal directions (for example, the three principal directions), where $\overline{\boldsymbol{\mu}}_{tt}(\boldsymbol{\beta} \to 0, \omega)$ is determined by solving the microscopic equations for the macroscopic fields of the fundamental Floquet-mode of the 3D array. If $|k_0 d|$ is sufficiently small (and $\boldsymbol{\beta} \to 0$), the array behaves as a continuum and the complete dyadic $\overline{\boldsymbol{\mu}}_b(0, \omega)$ is the $\boldsymbol{\beta} = 0$ continuum permeability dyadic which gives the three-component continuum $\mathbf{H}_b$ field in terms of the three components of the continuum $\mathbf{B}_b$ field by means of the constitutive relationship in (45), provided the inclusion material is not bianisotropic for small $|k_0 d|$ as $\boldsymbol{\beta} \to 0$ [21]. Also, the permeability often varies by a small amount with $\boldsymbol{\beta}$ for $|\boldsymbol{\beta} d| \ll 1$ and then the relationships in (51) hold approximately over the bandwidths of $|\boldsymbol{\beta} d| \ll 1$ and $|k_0 d| \ll 1$.

For the permittivity dyadics, the equations analogous to (51) can be used to determine $\overline{\boldsymbol{\epsilon}}_b(0, \omega)$ exactly for all ω, even for bianisotropic inclusions, from $\overline{\boldsymbol{\epsilon}}_{tt}(\boldsymbol{\beta} \to 0, \omega) = \overline{\boldsymbol{\epsilon}}_{ett}(\boldsymbol{\beta} \to 0, \omega)$ (and approximately for $|\boldsymbol{\beta} d| \ll 1$).

4. Reality and passivity conditions, reciprocity and causality relations for the spatially dispersive constitutive parameters

The definitions of the spatially dispersive macroscopic fields and constitutive parameters for the fundamental Floquet modes are similar, though not identical, to those in a spatially nondispersive continuum. Consequently, we find in this section that the reality conditions, reciprocity relations, passivity conditions, and causality relations for the fundamental Floquet modes also differ from their corresponding spatially nondispersive continuum relationships. Nevertheless, as the spatial and temporal frequencies, $\boldsymbol{\beta}$ and ω, become sufficiently small for the arrays to approximate continua, then the reality conditions, reciprocity relations, and passivity conditions become essentially the same as those of a spatially nondispersive dipolar continuum.

4.1. Reality conditions

The reality conditions for the fundamental Floquet modes of an array can be derived by returning to the applied current density in (7). Although the space–time fields and sources associated with (4)–(6) are real, we have assumed a complex plane-wave source in (7). Thus, an unstated assumption in (7) is that corresponding to each plane wave there is another plane wave $\mathbf{J}_a(-\boldsymbol{\beta}, -\omega)e^{-i(\boldsymbol{\beta}\cdot\mathbf{r}-\omega t)}$ such that

$$\mathbf{J}_a(\boldsymbol{\beta}, \omega)e^{i(\boldsymbol{\beta}\cdot\mathbf{r}-\omega t)} + \mathbf{J}_a(-\boldsymbol{\beta}, -\omega)e^{-i(\boldsymbol{\beta}\cdot\mathbf{r}-\omega t)} \tag{52}$$

is a real valued current-density function of $\mathbf{r}$ and t. Since this space–time vector is real valued, taking the complex conjugate of (52) does not change its value. It follows that

$$\mathbf{J}_a(-\boldsymbol{\beta}, -\omega) = \mathbf{J}_a^*(\boldsymbol{\beta}, \omega) \tag{53}$$

and similarly for the other fundamental Floquet-mode source and field vectors in (42) and (44). Also, it follows from the constitutive relations in (39), (41), and (44a) that

$$\overline{\boldsymbol{\epsilon}}_e(-\boldsymbol{\beta}, -\omega) = \overline{\boldsymbol{\epsilon}}_e^*(\boldsymbol{\beta}, \omega) \tag{54a}$$

$$\overline{\boldsymbol{\epsilon}}(-\boldsymbol{\beta},-\omega)=\overline{\boldsymbol{\epsilon}}^{*}(\boldsymbol{\beta},\omega) \tag{54b}$$

$$\overline{\boldsymbol{\mu}}_{tt}(-\boldsymbol{\beta},-\omega)=\overline{\boldsymbol{\mu}}_{tt}^{*}(\boldsymbol{\beta},\omega)\,. \tag{54c}$$

The anisotropic constitutive parameters satisfy the same kind of reality relation as the fields.

4.2. Reciprocity relations

To derive general reciprocity relations for the spatially dispersive constitutive parameters of the fundamental Floquet modes, begin with the Maxwell space–frequency domain equations in (4a) and (4b) for an array of lossy or lossless polarizable inclusions with applied electric current density given in (7) and the same equations but with $-\boldsymbol{\beta}$ replacing $\boldsymbol{\beta}$. Taking the dot product of $\boldsymbol{\mathcal{B}}_{\omega}^{-}(\mathbf{r})/\mu_0$, $\boldsymbol{\mathcal{E}}_{\omega}^{-}(\mathbf{r})$, $\boldsymbol{\mathcal{B}}_{\omega}(\mathbf{r})/\mu_0$, and $\boldsymbol{\mathcal{E}}_{\omega}(\mathbf{r})$ with these equations, then integrating over a unit cell and applying the divergence theorem gives [21]

$$\begin{aligned}0=&\left[\mathbf{J}_{\mathrm{a}}(\boldsymbol{\beta},\omega)\cdot\mathbf{E}(-\boldsymbol{\beta},\omega)-\mathbf{J}_{\mathrm{a}}(-\boldsymbol{\beta},\omega)\cdot\mathbf{E}(\boldsymbol{\beta},\omega)\right]+\\&\frac{1}{d^3}\int_{V_c}\left\{\left[\boldsymbol{\mathcal{J}}_{\omega}^{p}(\mathbf{r})\cdot\boldsymbol{\mathcal{E}}_{\omega}^{-}(\mathbf{r})-\boldsymbol{\mathcal{J}}_{\omega}^{p-}(\mathbf{r})\cdot\boldsymbol{\mathcal{E}}_{\omega}(\mathbf{r})\right]\right.\\&\left.+i\omega\left[\boldsymbol{\mathcal{M}}_{\omega}(\mathbf{r})\cdot\boldsymbol{\mathcal{B}}_{\omega}^{-}(\mathbf{r})-\boldsymbol{\mathcal{M}}_{\omega}^{-}(\mathbf{r})\cdot\boldsymbol{\mathcal{B}}_{\omega}(\mathbf{r})\right]\right\}d^3r\end{aligned} \tag{55}$$

where the superscripts "$-$" denotes the $-\boldsymbol{\beta}$ fields.

The next step in determining the reciprocity relations for the constitutive parameters is to prove that the integral in (55) is zero for arrays with lossy or lossless polarizable inclusions made of linear reciprocal material. Assuming a general linear bianisotropic relationship between $[\boldsymbol{\mathcal{J}}_{\omega}^{p}(\mathbf{r}),\boldsymbol{\mathcal{M}}_{\omega}(\mathbf{r})]$ and $[\boldsymbol{\mathcal{E}}_{\omega}(\mathbf{r}),\boldsymbol{\mathcal{B}}_{\omega}(\mathbf{r})]$ for the inclusions of the array, one can write

$$\begin{aligned}\boldsymbol{\mathcal{J}}_{\omega}^{p}(\mathbf{r})=&\int_{V_c}\left[\overline{\boldsymbol{\sigma}}_{\omega}^{e}(\mathbf{r},\mathbf{r}')\cdot\boldsymbol{\mathcal{E}}_{\omega}(\mathbf{r}')+\overline{\boldsymbol{\sigma}}_{\omega}^{em}(\mathbf{r},\mathbf{r}')\right.\\&\left.\cdot\boldsymbol{\mathcal{B}}_{\omega}(\mathbf{r}')\right]d^3r'\end{aligned} \tag{56a}$$

$$\begin{aligned}\boldsymbol{\mathcal{M}}_{\omega}(\mathbf{r})=&\int_{V_c}\left[\overline{\boldsymbol{\sigma}}_{\omega}^{m}(\mathbf{r},\mathbf{r}')\cdot\boldsymbol{\mathcal{B}}_{\omega}(\mathbf{r}')+\overline{\boldsymbol{\sigma}}_{\omega}^{me}(\mathbf{r},\mathbf{r}')\right.\\&\left.\cdot\boldsymbol{\mathcal{E}}_{\omega}(\mathbf{r}')\right]d^3r'\end{aligned} \tag{56b}$$

and similarly for the $-\boldsymbol{\beta}$ fields where the spatially dispersive microscopic "conductivity" dyadics, $\overline{\boldsymbol{\sigma}}_{\omega}^{e}(\mathbf{r},\mathbf{r}')$, $\overline{\boldsymbol{\sigma}}_{\omega}^{m}(\mathbf{r},\mathbf{r}')$, $\overline{\boldsymbol{\sigma}}_{\omega}^{em}(\mathbf{r},\mathbf{r}')$, and $\overline{\boldsymbol{\sigma}}_{\omega}^{me}(\mathbf{r},\mathbf{r}')$, are zero for $\mathbf{r}$ or $\mathbf{r}'$ outside the material of the inclusion. For simply "conducting" inclusions, $\overline{\boldsymbol{\sigma}}_{\omega}=\sigma^{e}\overline{\mathbf{I}}$, $\overline{\boldsymbol{\sigma}}_{\omega}^{m}=\sigma^{m}\overline{\mathbf{I}}$, and $\overline{\boldsymbol{\sigma}}_{\omega}^{em}=\overline{\boldsymbol{\sigma}}_{\omega}^{me}=0$, where σ^{e} and σ^{m} are scalar constants.

Insertion of the fields from (56) and the similar fields for $-\boldsymbol{\beta}$ into the integral of (55) yields

$$\mathbf{J}_{\mathrm{a}}(\boldsymbol{\beta},\omega)\cdot\mathbf{E}(-\boldsymbol{\beta},\omega)-\mathbf{J}_{\mathrm{a}}(-\boldsymbol{\beta},\omega)\cdot\mathbf{E}(\boldsymbol{\beta},\omega)=0 \tag{57}$$

after assuming that the inclusion material is reciprocal, that is

$$\overline{\boldsymbol{\sigma}}_{\omega}(\mathbf{r}',\mathbf{r})=\overline{\boldsymbol{\sigma}}_{\omega}^{e\mathrm{T}}(\mathbf{r}',\mathbf{r}) \tag{58a}$$

$$\overline{\boldsymbol{\sigma}}_{\omega}^{m}(\mathbf{r},\mathbf{r}')=\overline{\boldsymbol{\sigma}}_{\omega}^{m\mathrm{T}}(\mathbf{r}',\mathbf{r}) \tag{58b}$$

$$\overline{\boldsymbol{\sigma}}_{\omega}^{em}(\mathbf{r},\mathbf{r}')=\overline{\boldsymbol{\sigma}}_{\omega}^{me\mathrm{T}}(\mathbf{r}',\mathbf{r})\,. \tag{58c}$$

Substitute $\mathbf{J}_{\mathrm{a}}(\boldsymbol{\beta},\omega)$ and $\mathbf{J}_{\mathrm{a}}(-\boldsymbol{\beta},\omega)$ from (42b) into (57), and $\mathbf{B}(\boldsymbol{\beta},\omega)$ and $\mathbf{B}(-\boldsymbol{\beta},\omega)$ from (42a) to obtain

$$\begin{aligned}&\mathbf{E}(-\boldsymbol{\beta},\omega)\cdot\left\{\left[\overline{\boldsymbol{\epsilon}}(\boldsymbol{\beta},\omega)+\frac{\overline{\boldsymbol{\beta}}}{\omega^2}\cdot\overline{\boldsymbol{\mu}}_{tt}^{-1}(\boldsymbol{\beta},\omega)\cdot\overline{\boldsymbol{\beta}}\right]\right.\\&\left.-\left[\overline{\boldsymbol{\epsilon}}(-\boldsymbol{\beta},\omega)+\frac{\overline{\boldsymbol{\beta}}}{\omega^2}\cdot\overline{\boldsymbol{\mu}}_{tt}^{-1}(-\boldsymbol{\beta},\omega)\cdot\overline{\boldsymbol{\beta}}\right]^{\mathrm{T}}\right\}\cdot\mathbf{E}(\boldsymbol{\beta},\omega)=0.\end{aligned} \tag{59}$$

The antisymmetric dyadic $\overline{\boldsymbol{\beta}}$ is used to replace $\boldsymbol{\beta}\times$; that is, $\overline{\boldsymbol{\beta}}\cdot\mathbf{V}=-\mathbf{V}\cdot\overline{\boldsymbol{\beta}}=\boldsymbol{\beta}\times\mathbf{V}=-\mathbf{V}\times\boldsymbol{\beta}$ for any vector $\mathbf{V}$, and the superscript "T" denotes the transpose. The bilinear form in (59) has to be zero for all values of $\mathbf{E}(\boldsymbol{\beta},\omega)$ and $\mathbf{E}(-\boldsymbol{\beta},\omega)$. Thus, we find the following reciprocity relation for the anisotropic constitutive dyadics of 3D arrays of linear, reciprocal bianisotropic lossy or lossless polarizable inclusions at all real values of $(\boldsymbol{\beta},\omega)$

$$\begin{aligned}&\left[\overline{\boldsymbol{\epsilon}}(\boldsymbol{\beta},\omega)+\frac{1}{\omega^2}\overline{\boldsymbol{\beta}}\cdot\overline{\boldsymbol{\mu}}_{tt}^{-1}(\boldsymbol{\beta},\omega)\cdot\overline{\boldsymbol{\beta}}\right]\\&=\left[\overline{\boldsymbol{\epsilon}}(-\boldsymbol{\beta},\omega)+\frac{1}{\omega^2}\overline{\boldsymbol{\beta}}\cdot\overline{\boldsymbol{\mu}}_{tt}^{-1}(-\boldsymbol{\beta},\omega)\cdot\overline{\boldsymbol{\beta}}\right]^{\mathrm{T}}.\end{aligned} \tag{60}$$

If we had applied the Landau–Lifshitz single polarization formulation [2,11,14] discussed in Section 1 to the fundamental Floquet modes, $i\omega\mathbf{D}$ in (24b) would include $-i\boldsymbol{\beta}\times(\mathbf{M}^{e}+\mathbf{M})$ so that $\mathbf{H}=\mathbf{B}/\mu_0$ and $\mathbf{D}=\overline{\boldsymbol{\epsilon}}_{L}\cdot\mathbf{E}$, where

$$\overline{\boldsymbol{\epsilon}}_{L}(\boldsymbol{\beta},\omega)=\overline{\boldsymbol{\epsilon}}(\boldsymbol{\beta},\omega)+\frac{1}{\omega^2}\overline{\boldsymbol{\beta}}\cdot\left[\overline{\boldsymbol{\mu}}_{tt}^{-1}(\boldsymbol{\beta},\omega)-\mu_0^{-1}\overline{\mathbf{I}}\right]\cdot\overline{\boldsymbol{\beta}}. \tag{61}$$

Then we see that (60) expresses the single-polarization reciprocity relation [2,11,14]

$$\overline{\boldsymbol{\epsilon}}_{L}(\boldsymbol{\beta},\omega)=\overline{\boldsymbol{\epsilon}}_{L}^{\mathrm{T}}(-\boldsymbol{\beta},\omega) \tag{62}$$

which, except for the $-\boldsymbol{\beta}$, has the form of the conventional permittivity reciprocity relation in spatially nondispersive continuous media [19, p. 403]. Note,

however, that for the fundamental Floquet modal equations, the proof of the reciprocity relations in (60) and (62) has required returning to the basic definition of reciprocity in the microscopic Maxwellian equations describing the material of the inclusions of the array. Although the Landau–Lifshitz single constitutive dyadic $\overline{\boldsymbol{\epsilon}}_L(\boldsymbol{\beta},\omega)$ for a continuum can be formally expressed as in (61) in terms of effective multipole-moment permittivity and permeability dyadics for the continuum [35], the continuum formulation does not provide microscopic expressions as in (20) needed to determine $\overline{\boldsymbol{\epsilon}}(\boldsymbol{\beta},\omega)$ and $\overline{\boldsymbol{\mu}}_{tt}(\boldsymbol{\beta},\omega)$.

Letting $\boldsymbol{\beta}\to 0$ in (60) reveals that

$$\overline{\boldsymbol{\epsilon}}(0,\omega)=\overline{\boldsymbol{\epsilon}}^{\mathrm{T}}(0,\omega) \tag{63a}$$

or more generally

$$\overline{\boldsymbol{\epsilon}}(\boldsymbol{\beta},\omega)\approx\overline{\boldsymbol{\epsilon}}^{\mathrm{T}}(-\boldsymbol{\beta},\omega),\qquad |\boldsymbol{\beta}d|\ll 1\,. \tag{63b}$$

It does not necessarily follow from (60) that the permeability $\overline{\boldsymbol{\mu}}_{tt}(\boldsymbol{\beta}\to 0,\omega)$ satisfies the same reciprocity relation as $\overline{\boldsymbol{\epsilon}}(0,\omega)$ in (63). However, for both $|\boldsymbol{\beta}d|\ll 1$ and $|k_0 d|\ll 1$, the permittivity and inverse permeability dyadics are finite continuous functions of $\boldsymbol{\beta}$ and ω for nonbianisotropic inclusions, and the inverse permeability varies as $\omega/|\boldsymbol{\beta}|$ for bianisotropic inclusions [21]. Thus by varying the ratio of $\boldsymbol{\beta}/\omega$ in (59), the $\overline{\boldsymbol{\epsilon}}$ and $\overline{\boldsymbol{\mu}}_{tt}^{-1}$ terms have to obey (59) separately to give from the $\overline{\boldsymbol{\mu}}_{tt}^{-1}$ term

$$\overline{\boldsymbol{\mu}}_{tt}^{-1}(\boldsymbol{\beta},\omega)\approx\overline{\boldsymbol{\mu}}_{tt}^{-1\mathrm{T}}(-\boldsymbol{\beta},\omega),\quad (|\boldsymbol{\beta}d|\ll 1,|k_0 d|\ll 1) \tag{64a}$$

or

$$\overline{\boldsymbol{\mu}}_{tt}(\boldsymbol{\beta},\omega)\approx\overline{\boldsymbol{\mu}}_{tt}^{\mathrm{T}}(-\boldsymbol{\beta},\omega),\quad (|\boldsymbol{\beta}d|\ll 1,|k_0 d|\ll 1) \tag{64b}$$

for reciprocal arrays and $\boldsymbol{\beta}/\omega\neq 0$ in (64a) if the inclusions are bianisotropic at the low spatial and temporal frequencies. Unlike the complete dyadics, $\overline{\boldsymbol{\epsilon}}(0,\omega)$ and $\overline{\boldsymbol{\mu}}_{\mathrm{b}}(0,\omega)$, the elements of the transverse dyadic $\overline{\boldsymbol{\mu}}_{tt}(\boldsymbol{\beta}\to 0,\omega)$ can depend on the direction of $\boldsymbol{\beta}$ as $\boldsymbol{\beta}\to 0$. The complete permeability dyadic $\overline{\boldsymbol{\mu}}_{\mathrm{b}}(0,\omega)$ is given in terms of the transverse dyadic $\overline{\boldsymbol{\mu}}_{tt}(\boldsymbol{\beta}\to 0,\omega)$ in (51) except possibly for bianisotropic inclusions, which yield a singular $\overline{\boldsymbol{\mu}}_{tt}^{-1}(\boldsymbol{\beta},\omega)$ as $\boldsymbol{\beta}/\omega\to 0$ [21]. Thus, as explained in Section 1, a bianisotropic formulation [16,18] of metamaterials comprised of bianisotropic inclusions may be more suitable than an anisotropic formulation especially for small values of $\boldsymbol{\beta}$ and ω.

4.3. Passivity conditions

Passivity conditions obeyed by the permittivity and permeability constitutive dyadics of the fundamental Floquet modes of passive (no internal sources of power within the material of the inclusions) arrays can be found from the expression for the time-average power supplied by the microscopic electric field $\boldsymbol{\mathcal{E}}_\omega(\mathbf{r})$ to the applied electric current density of (7) in each unit cell. This time-average power has to be equal to or less than zero or else average power could be extracted from the passive array; specifically

$$\frac{1}{2}\mathrm{Re}\int_{V_c}\mathbf{J}_{\mathrm{a}}(\boldsymbol{\beta},\omega)\cdot\boldsymbol{\mathcal{E}}_\omega^*(\mathbf{r})e^{i\boldsymbol{\beta}\cdot\mathbf{r}}d^3r\le 0 \tag{65}$$

where, as usual, the superscript "*" denotes the complex conjugate. The inequality in (65) holds for lossy inclusion material, while the equality holds for lossless inclusion material. Insertion of $\boldsymbol{\mathcal{E}}_\omega^*(\mathbf{r})$ from (8) re-expresses (65) in terms of the fundamental Floquet modal spectra as

$$\mathrm{Re}[\mathbf{J}_{\mathrm{a}}(\boldsymbol{\beta},\omega)\cdot\mathbf{E}^*(\boldsymbol{\beta},\omega)]\le 0 \tag{66}$$

in which the superfluous factor $d^3/2$ has been omitted. (This equation shows that all the power supplied by the applied electric current density can be expressed in terms of the fundamental Floquet modal spectra $\mathbf{J}_{\mathrm{a}}$ and $\mathbf{E}$. Higher order Floquet modal spectra are not required.)

With $\mathbf{J}_{\mathrm{a}}$ substituted from (42b) into (66), then $\mathbf{B}$ substituted from (42a), we find

$$\omega\mathrm{Im}\left\{\mathbf{E}^*\cdot\left[\overline{\boldsymbol{\epsilon}}+\frac{1}{\omega^2}\overline{\boldsymbol{\beta}}\cdot\overline{\boldsymbol{\mu}}_{tt}^{-1}\cdot\overline{\boldsymbol{\beta}}\right]\cdot\mathbf{E}\right\}\ge 0. \tag{67}$$

Since (67) has to hold for all values of $\mathbf{E}$, the array is passive and lossy, or passive and lossless, if and only if its associated Hermitian "loss" matrix is positive definite (PD) or zero [36], respectively; that is

$$-i\omega\left[\left(\overline{\boldsymbol{\epsilon}}(\boldsymbol{\beta},\omega)+\frac{1}{\omega^2}\overline{\boldsymbol{\beta}}\cdot\overline{\boldsymbol{\mu}}_{tt}^{-1}(\boldsymbol{\beta},\omega)\cdot\overline{\boldsymbol{\beta}}\right)-\left(\overline{\boldsymbol{\epsilon}}(\boldsymbol{\beta},\omega)+\frac{1}{\omega^2}\overline{\boldsymbol{\beta}}\cdot\overline{\boldsymbol{\mu}}_{tt}^{-1}(\boldsymbol{\beta},\omega)\cdot\overline{\boldsymbol{\beta}}\right)^{*\mathrm{T}}\right]=\mathrm{PD} \tag{68a}$$

for lossy material, and[4]

$$\left[\overline{\boldsymbol{\epsilon}}(\boldsymbol{\beta},\omega)+\frac{1}{\omega^2}\overline{\boldsymbol{\beta}}\cdot\overline{\boldsymbol{\mu}}_{tt}^{-1}(\boldsymbol{\beta},\omega)\cdot\overline{\boldsymbol{\beta}}\right] \tag{68b}$$

[4] At unit-cell resonant frequencies ($\omega=\omega_{\mathrm{uc}}(\boldsymbol{\beta})$) of lossless arrays, the $\mathbf{E}(\boldsymbol{\beta},\omega_{\mathrm{uc}})$ and $\mathbf{B}(\boldsymbol{\beta},\omega_{\mathrm{uc}})$ can be zero and the permittivity and inverse permeability can have poles. Thus, (68b) does not necessarily hold at these unit-cell resonant frequencies. These unit-cell singularities disappear for real values of $\boldsymbol{\beta}$ and ω if a small loss is inserted into the material of the array inclusions.

$$= \left[\overline{\boldsymbol{\epsilon}}(\boldsymbol{\beta},\omega) + \frac{1}{\omega^2}\overline{\boldsymbol{\beta}}\cdot\overline{\boldsymbol{\mu}}_{tt}^{-1}(\boldsymbol{\beta},\omega)\cdot\overline{\boldsymbol{\beta}}\right]^{*\mathrm{T}}, \quad \omega \neq \omega_{\mathrm{uc}}$$

for lossless material. For scalar permittivity and permeability transverse to $\boldsymbol{\beta}$ (that is, $\overline{\boldsymbol{\epsilon}} = \epsilon\overline{\mathbf{I}}_{tt}$ and $\overline{\boldsymbol{\mu}}_{tt} = \mu\overline{\mathbf{I}}_{tt}$), (68) reduce to

$$\omega\mathrm{Im}\left[\epsilon(\boldsymbol{\beta},\omega) - \frac{|\boldsymbol{\beta}|^2}{\omega^2\mu(\boldsymbol{\beta},\omega)}\right] > 0 \tag{69a}$$

$$\mathrm{Im}\left[\epsilon(\boldsymbol{\beta},\omega) - \frac{|\boldsymbol{\beta}|^2}{\omega^2\mu(\boldsymbol{\beta},\omega)}\right] = 0, \qquad \omega \neq \omega_{\mathrm{uc}} \tag{69b}$$

in lossy and lossless inclusion material, respectively. These conditions do not necessarily imply that the imaginary parts of ϵ and μ are equal to or greater than zero, or even that the imaginary parts of ϵ and μ are zero in lossless arrays. In general, (69b) shows only that the imaginary parts of ϵ and μ have opposite signs in lossless arrays such that the total power dissipated by the array is zero. From (61) it is seen that in terms of the Landau–Lifshitz single polarization formulation [2,11,14], the lossy and lossless conditions in (68) reduce, respectively, to

$$-i\omega\left[\overline{\boldsymbol{\epsilon}}_L(\boldsymbol{\beta},\omega) - \overline{\boldsymbol{\epsilon}}_L^{*\mathrm{T}}(\boldsymbol{\beta},\omega)\right] = \mathrm{PD} \qquad \text{(lossy)} \tag{70a}$$

$$\overline{\boldsymbol{\epsilon}}_L(\boldsymbol{\beta},\omega) = \overline{\boldsymbol{\epsilon}}_L^{*\mathrm{T}}(\boldsymbol{\beta},\omega), \qquad \omega \neq \omega_{\mathrm{uc}} \qquad \text{(lossless)}. \tag{70b}$$

As with the reciprocity relations for the fundamental Floquet modal equations, the proof of these lossy–lossless conditions has required returning to the basic definition of loss and losslessness in the microscopic Maxwellian equations describing the material of the inclusions of the array. Also, as mentioned in Section 4.2, although the Landau–Lifshitz single constitutive dyadic $\overline{\boldsymbol{\epsilon}}_L(\boldsymbol{\beta},\omega)$ for a continuum can be formally expressed as in (61) in terms of effective multipole-moment permittivity and permeability dyadics for the continuum [35], the continuum formulation does not provide microscopic expressions as in (20) needed to determine $\overline{\boldsymbol{\epsilon}}(\boldsymbol{\beta},\omega)$ and $\overline{\boldsymbol{\mu}}_{tt}(\boldsymbol{\beta},\omega)$.

Letting $\boldsymbol{\beta} \to 0$ in (68) reveals that

$$-i\omega\left[\overline{\boldsymbol{\epsilon}}(0,\omega) - \overline{\boldsymbol{\epsilon}}^{*\mathrm{T}}(0,\omega)\right] = \mathrm{PD} \qquad \text{(lossy)} \tag{71a}$$

$$\overline{\boldsymbol{\epsilon}}(0,\omega) = \overline{\boldsymbol{\epsilon}}^{*\mathrm{T}}(0,\omega), \qquad \omega \neq \omega_{\mathrm{uc}} \qquad \text{(lossless)} \tag{71b}$$

for lossy and lossless arrays, respectively. These equations imply

$$\omega\mathrm{Im}[\epsilon_{jj}(0,\omega)] > 0 \qquad \text{(lossy)} \tag{71c}$$

$$\epsilon_{jk}(0,\omega) = \epsilon_{kj}^*(0,\omega), \qquad \omega \neq \omega_{\mathrm{uc}} \qquad \text{(lossless)} \tag{71d}$$

for lossy and lossless arrays, respectively. The lossy–lossless passivity conditions in (71) have the same form as the lossy–lossless passivity conditions on permittivity in a spatially nondispersive dipolar continuum. They also hold approximately for $|\boldsymbol{\beta}d| \ll 1$.

It does not necessarily follow from (68) that $\overline{\boldsymbol{\mu}}_{tt}(\boldsymbol{\beta}\to 0,\omega)$ satisfies the same passivity conditions as $\overline{\boldsymbol{\epsilon}}(0,\omega)$ in (71). However, for both $|\boldsymbol{\beta}d| \ll 1$ and $|k_0 d| \ll 1$, the permittivity and inverse permeability dyadics are finite continuous functions of $\boldsymbol{\beta}$ and ω for nonbianisotropic inclusions, and the inverse permeability varies as $\boldsymbol{\beta}/\omega$ for bianisotropic inclusions [21]. Thus, by varying the ratio of $\boldsymbol{\beta}/\omega$ in (67), the $\overline{\boldsymbol{\epsilon}}$ and $\overline{\boldsymbol{\mu}}_{tt}^{-1}$ terms have to obey (67) independently to give for the $\overline{\boldsymbol{\mu}}_{tt}^{-1}$ term

$$i\omega[\mathbf{E}\cdot\overline{\boldsymbol{\beta}}]^*\cdot[\overline{\boldsymbol{\mu}}_{tt}^{-1} - \overline{\boldsymbol{\mu}}_{tt}^{-1*\mathrm{T}}]\cdot[\mathbf{E}\cdot\overline{\boldsymbol{\beta}}] \geq 0 \tag{72}$$

which implies

$$i\omega[\overline{\boldsymbol{\mu}}_{tt}^{-1} - \overline{\boldsymbol{\mu}}_{tt}^{-1*\mathrm{T}}] = \mathrm{PD}, \quad (|\boldsymbol{\beta}d|, |k_0 d|) \ll 1 \quad \text{(lossy)} \tag{73a}$$

$$\overline{\boldsymbol{\mu}}_{tt} \approx \overline{\boldsymbol{\mu}}_{tt}^{*\mathrm{T}}, \quad (|\boldsymbol{\beta}d|, |k_0 d|) \ll 1 \quad \text{(lossless)} \tag{73b}$$

$$\omega\mathrm{Im}[\mu_{ttjj}] > 0, \quad (|\boldsymbol{\beta}d|, |k_0 d|) \ll 1 \quad \text{(lossy)} \tag{73c}$$

$$\mu_{ttjk} = \mu_{ttkj}^*, \quad (|\boldsymbol{\beta}d|, |k_0 d|) \ll 1 \quad \text{(lossless)} \tag{73d}$$

for passive inclusions and $\boldsymbol{\beta}/\omega \neq 0$ in (73a) if the inclusions are bianisotropic at the low spatial and temporal frequencies. Unlike $\overline{\boldsymbol{\epsilon}}(0,\omega)$, the permeability dyadic $\overline{\boldsymbol{\mu}}_{tt}(\boldsymbol{\beta}\to 0,\omega)$ does not necessarily satisfy these passivity conditions for lossy or lossless arrays if $\not<$. Also, unlike the complete dyadics, $\overline{\boldsymbol{\epsilon}}(0,\omega)$ and $\overline{\boldsymbol{\mu}}_{\mathrm{b}}(0,\omega)$, the elements of the transverse dyadic $\overline{\boldsymbol{\mu}}_{tt}(\boldsymbol{\beta}\to 0,\omega)$ can depend on the direction of $\boldsymbol{\beta}$ as $\boldsymbol{\beta}\to 0$. The complete permeability dyadic $\overline{\boldsymbol{\mu}}_{\mathrm{b}}(0,\omega)$ is given in terms of the transverse dyadic $\overline{\boldsymbol{\mu}}_{tt}(\boldsymbol{\beta}\to 0,\omega)$ in (51) except possibly for bianisotropic inclusions, which yield a singular $\overline{\boldsymbol{\mu}}_{\mathrm{tt}}^{-1}(\boldsymbol{\beta},\omega)$ as $\boldsymbol{\beta}/\omega \to 0$ [21]. Thus, as explained in Section 1, a bianisotropic formulation [16,18] of metamaterials comprised of bianisotropic inclusions may be more suitable than an anisotropic formulation especially for small values of $\boldsymbol{\beta}$ and ω.

4.4. Causality relations

To discuss the causality of the macroscopic permittivity and inverse-permeability dyadics, $\overline{\boldsymbol{\epsilon}}(\boldsymbol{\beta},\omega)$ and $\overline{\boldsymbol{\mu}}_{tt}^{-1}(\boldsymbol{\beta},\omega)$, begin by taking the four-fold $(\boldsymbol{\beta}, \omega)$ Fourier transform of the fundamental Floquet-mode constitutive relation in (39) and use the convolution

theorem to obtain

$$\mathcal{D}_0(\mathbf{r},t) = \frac{1}{(2\pi)^4}\int\int\int\int_{-\infty}^{+\infty}\overline{\varepsilon}_0(\mathbf{r}',t') \cdot\mathcal{E}_0(\mathbf{r}-\mathbf{r}',t-t')d^3r'dt' \tag{74}$$

in which the time-domain functions are the inverse Fourier transforms of the corresponding frequency-domain functions; in particular

$$\overline{\varepsilon}_0(\mathbf{r},t) = \int\int\int\int_{-\infty}^{+\infty}\overline{\boldsymbol{\epsilon}}_e(\boldsymbol{\beta},\omega)e^{i(\boldsymbol{\beta}\cdot\mathbf{r}-\omega t)}d^3\beta d\omega. \tag{75}$$

The functions of $(\mathbf{r}, t)$ in (74)–(75) are real because of the reality conditions satisfied by the spectra.

The function $\mathcal{E}_0(\mathbf{r},t)$ is the total time-domain electric field of the fundamental Floquet mode, which is excited by time-domain externally applied electric current density $\mathcal{J}_{a0}(\mathbf{r},t)$ that we shall stipulate turns on at $t = 0$. Assuming that the material of the inclusions is causal or, more precisely, that the linear constitutive parameters of the inclusion material are causal, the induced fields in the inclusions cannot begin before the applied current and thus the total electric field (induced plus applied) begins at $t = 0$. Since the generalized time-domain displacement vector $\mathcal{D}_0(\mathbf{r},t)$ is a linear combination of the total electric field of the fundamental Floquet mode and the induced generalized electric polarization as given in (23a), and this induced polarization cannot begin before the applied electric field begins at $t = 0$, it follows that $\mathcal{D}_0(\mathbf{r},t)$ must be zero for $t < 0$. This implies from (74) that $\overline{\varepsilon}_0(\mathbf{r},t) = 0$ for $t < 0$, so that we have from (75)

$$\overline{\varepsilon}_0(\mathbf{r},t) = \int\int\int\int_{-\infty}^{+\infty}\overline{\boldsymbol{\epsilon}}_e(\boldsymbol{\beta},\omega)e^{i(\boldsymbol{\beta}\cdot\mathbf{r}-\omega t)}d^3\beta d\omega = 0, \quad t<0. \tag{76}$$

Taking the three $\boldsymbol{\beta}$ Fourier transforms of (76) yields the following fundamental causality relation on $\overline{\boldsymbol{\epsilon}}_e(\boldsymbol{\beta},\omega)$ for each real value of $\boldsymbol{\beta}$

$$\int_{-\infty}^{+\infty}\overline{\boldsymbol{\epsilon}}_e(\boldsymbol{\beta},\omega)e^{-i\omega t}d\omega = 0, \quad t<0. \tag{77a}$$

A similar argument beginning with (41) instead of (39), and noting that $\mathbf{B}$ and $\mathbf{E}_l$ in (41) are primary fields that can be chosen independently, yields the analogous causality relation for the inverse permeability

$$\int_{-\infty}^{+\infty}\overline{\boldsymbol{\mu}}_{tt}^{-1}(\boldsymbol{\beta},\omega)e^{-i\omega t}d\omega = 0, \quad t<0 \tag{77b}$$

and the analogous causality relation for the magneto-electric constitutive parameter $\overline{\boldsymbol{\nu}}_{tl}(\boldsymbol{\beta},\omega)$ in (41). Having obtained the causality of $\overline{\boldsymbol{\epsilon}}_e$ and $\overline{\boldsymbol{\nu}}_{tl}$, it follows from (43) that $\overline{\boldsymbol{\epsilon}}(\boldsymbol{\beta},\omega)$ is also a causal function satisfying

$$\int_{-\infty}^{+\infty}\overline{\boldsymbol{\epsilon}}(\boldsymbol{\beta},\omega)e^{-i\omega t}d\omega = 0, \quad t<0. \tag{77c}$$

An especially attractive feature of the Floquet modal representation developed here is that the above argument for causality holds because none of the integrally defined generalized electric and magnetic polarization densities for the fundamental Floquet mode are approximations. This stands in contrast, for example, to conventional formulations using electric and magnetic dipole approximations, which have been shown to be inherently noncausal, and thus do not satisfy either the basic causality relations in (77) or the Kramers–Kronig relations in (78); see [20].

Also, the causality relations for $\overline{\boldsymbol{\epsilon}}(\boldsymbol{\beta},\omega)$ and $\overline{\boldsymbol{\mu}}_{tt}^{-1}(\boldsymbol{\beta},\omega)$ in (77) always hold as long as the integrals in (77) exist (converge) since $\overline{\boldsymbol{\epsilon}}(\boldsymbol{\beta},\omega)$ and $\overline{\boldsymbol{\mu}}_{tt}^{-1}(\boldsymbol{\beta},\omega)$ are well defined at each fixed $\boldsymbol{\beta}$ for all ω; see Footnote (4). (If $\overline{\boldsymbol{\epsilon}}(\boldsymbol{\beta},\omega)$ and $\overline{\boldsymbol{\mu}}_{tt}^{-1}(\boldsymbol{\beta},\omega)$ approach constants $\overline{\boldsymbol{\epsilon}}_\infty(\boldsymbol{\beta})$ and $\overline{\boldsymbol{\mu}}_{tt\infty}^{-1}(\boldsymbol{\beta})$ as $\omega\to\infty$, then these constants can be subtracted from $\overline{\boldsymbol{\epsilon}}(\boldsymbol{\beta},\omega)$ and $\overline{\boldsymbol{\mu}}_{tt}^{-1}(\boldsymbol{\beta},\omega)$ in (77c) and (77b), respectively, as in (78), to ensure that the causality integrals converge.)

This universal causality does not necessarily hold for the constitutive parameters of the source-free (no applied current density) fundamental eigenmodes of arrays for which $\boldsymbol{\beta}$ is a function of ω because, even for a single eigenmode, $\boldsymbol{\beta}(\omega)$ may not be a single-valued function of ω for all ω and there may be frequency bands where the eigenmode ceases to exist. In addition, $\boldsymbol{\beta}(\omega)$ for an eigenmode is not generally a real function of ω for all ω even if the inclusions of the array are lossless [23], and it becomes problematic to define field and polarization integrals that produce constitutive parameters consistent with the complex $\boldsymbol{\beta}(\omega)$. Also, for source-free eigenmodes, it often proves advantageous to define anisotropic permittivity and permeability in terms of their relationships to the propagation constants and field impedances of each eigenmode [5,23,37] rather than in terms of the field and polarization integrals (weighted averages) as in (13) and (20), and thus one array would have multiply defined constitutive parameters, none of which would necessarily be causal.

As a consequence of the causality relations in (77), the permittivity and inverse permeability dyadics satisfy the Kramers–Kronig causality equations for each fixed $\boldsymbol{\beta}$. The familiar Kramers–Kronig relations can be found

by taking the real and imaginary parts of their compact complex version given as [1, p. 98]

$$\overline{\boldsymbol{\epsilon}}(\boldsymbol{\beta},\omega)-\overline{\boldsymbol{\epsilon}}_{\infty}(\boldsymbol{\beta})=\frac{i}{\pi}\int_{-\infty}^{+\infty}\frac{\overline{\boldsymbol{\epsilon}}(\boldsymbol{\beta},\nu)-\overline{\boldsymbol{\epsilon}}_{\infty}(\boldsymbol{\beta})}{\omega-\nu}d\nu \tag{78a}$$

$$\overline{\boldsymbol{\mu}}_{tt}^{-1}(\boldsymbol{\beta},\omega)-\overline{\boldsymbol{\mu}}_{tt\infty}^{-1}(\boldsymbol{\beta})=\frac{i}{\pi}\int_{-\infty}^{+\infty}\frac{\overline{\boldsymbol{\mu}}_{tt}^{-1}(\boldsymbol{\beta},\nu)-\overline{\boldsymbol{\mu}}_{tt\infty}^{-1}(\boldsymbol{\beta})}{\omega-\nu}d\nu \tag{78b}$$

where the lines through the integrals denote principal value integrations. These Kramers–Kronig causality relations assume that for a fixed value of $\boldsymbol{\beta}$

$$\lim_{|\omega|\to\infty}\overline{\boldsymbol{\epsilon}}(\boldsymbol{\beta},\omega)=\overline{\boldsymbol{\epsilon}}_{\infty}(\boldsymbol{\beta}) \tag{79a}$$

$$\lim_{|\omega|\to\infty}\overline{\boldsymbol{\mu}}_{tt}^{-1}(\boldsymbol{\beta},\omega)=\overline{\boldsymbol{\mu}}_{tt\infty}^{-1}(\boldsymbol{\beta}) \tag{79b}$$

and that $\overline{\boldsymbol{\epsilon}}(\boldsymbol{\beta},\omega)-\overline{\boldsymbol{\epsilon}}_{\infty}(\boldsymbol{\beta})$ and $\overline{\boldsymbol{\mu}}_{tt}^{-1}(\boldsymbol{\beta},\omega)-\overline{\boldsymbol{\mu}}_{tt\infty}^{-1}(\boldsymbol{\beta})$ approach zero fast enough as $|\omega|\to\infty$ for the integrals in (78) to exist. A sufficient condition for the principal value integrals to be well defined for all real ω is that $\overline{\boldsymbol{\epsilon}}(\boldsymbol{\beta},\omega)-\overline{\boldsymbol{\epsilon}}_{\infty}(\boldsymbol{\beta})$ and $\overline{\boldsymbol{\mu}}_{tt}^{-1}(\boldsymbol{\beta},\omega)-\overline{\boldsymbol{\mu}}_{tt\infty}^{-1}(\boldsymbol{\beta})$ be Hölder continuous [38, ch. 1].

In Section 4.3 it was found that passivity of the inclusion material did not necessarily imply that the imaginary parts of the diagonal elements of the macroscopic permittivity and permeability dyadics are greater than zero at every ($\boldsymbol{\beta}$, ω). Moreover, lossless inclusions do not necessarily imply that the imaginary parts of the diagonal elements of the macroscopic permittivity and permeability dyadics are zero at every ($\boldsymbol{\beta}$, ω). However, it was proven, as expressed in (71d), that as $\boldsymbol{\beta}\to 0$ the imaginary parts of the permittivity diagonal elements, $\mathrm{Im}[\epsilon_{jj}(0,\omega)]$, were equal to zero for lossless inclusions except at the unit-cell resonant frequencies where insertion of a small loss shows from (71c) that $\omega\mathrm{Im}[\epsilon_{jj}(0,\omega)]$ is greater than zero. Consequently, the Kramers–Kronig relation in (78a) can be used to prove for lossless arrays [2, sec. 84] and $\boldsymbol{\beta}\to 0$ that except at the unit-cell resonant frequencies, the diagonal elements of the permittivity dyadic satisfy the inequalities

$$\frac{\partial[\omega\epsilon_{jj}(0,\omega)]}{\partial\omega}-\epsilon_{jj\,\infty}(0)\geq\frac{\omega}{2}\frac{\partial\epsilon_{jj}(0,\omega)}{\partial\omega}\geq 0,\quad \omega\neq\omega_{\mathrm{uc}}. \tag{80}$$

These same inequalities for $\mu_{ttjj}(\boldsymbol{\beta}\to 0,\ \omega)$ do not necessarily hold because, as explained in the context of Eqs. (73), the $\omega\mathrm{Im}[u_{ttjj}(\boldsymbol{\beta}\to 0,\ \omega)]$ may be <0 for $|k_0d|\ll 1$.

Lastly, we mention that the causality of an $\epsilon_{jj}(0,\omega)-\epsilon_{jj\,\infty}(0)$ expressed in (78a), coupled with the passivity condition in (71c), implies by means of the theorem proven in the Appendix of [21] that $\epsilon_{jj}^{-1}(0,\omega)-\epsilon_{jj\,\infty}^{-1}(0)$ is also a causal function. However, the causality of a $\mu_{ttjj}^{-1}(\boldsymbol{\beta}\to 0,\omega)-\mu_{ttjj\infty}^{-1}(\boldsymbol{\beta}\to 0)$ expressed in (78b) does not imply, by means of the theorem in this Appendix, the causality of $\mu_{ttjj}(\boldsymbol{\beta}\to 0,\omega)-\mu_{ttjj\infty}(\boldsymbol{\beta}\to 0)$ because $\mu_{ttjj}^{-1}(\boldsymbol{\beta}\to 0,\omega)$ does not necessarily satisfy the passivity condition in (73c) (with μ_{ttjj}^{-1} replacing μ_{ttjj} and "$>$" replacing "$<$") for all k_0d, that is, for all ω. In Section 5, we show a specific numerical example of an array having $\mu^{-1}(0,\omega)-\mu_{\infty}^{-1}(0)$ causal, whereas $\mu(0,\omega)-\mu_{\infty}(0)$ is not causal.

5. Numerical example

As a numerical example, we determine the macroscopic permittivity and permeability of a 2D metamaterial array, consisting of uniformly spaced, infinitely long dielectric circular cylinders, computed using a finite-difference frequency-domain (FDFD) solution to the rigorous equations derived in Sections 2–4. We limit the computations to $\boldsymbol{\beta}\to 0$ for the transverse solution with $\boldsymbol{\beta}=\beta\hat{\mathrm{z}}$ in a principal propagation direction z and the applied transverse electric current density $\mathbf{J}_{\mathrm{t}}=J_{\mathrm{t}}\hat{\mathrm{x}}$ normal to the plane formed by the principal propagation direction and the axial direction ($\hat{\mathrm{y}}$) of the cylinders. We choose a homogeneous, isotropic, causal, microscopic, Drude-model [30, ch. V], relative complex dielectric constant for each of the cylinders given by

$$\epsilon_{\mathrm{D}}=1-\frac{(k_pd)^2}{k_0d(k_0d+ik_cd)} \tag{81}$$

where d is the separation distance between the center of the circular cylinders located in free space on a square lattice, $k_0=\omega/c$, $k_pd=1.5$, $k_c=.05k_p$, and the radius a of each circular cylinder is chosen to be such that $a/d=0.40$. As $|\omega|\to\infty$, this relative complex dielectric constant approaches 1, and as $\omega\to 0$, it approaches $1+ik_p^2/(k_0k_c)$, the relative complex dielectric constant of an electrical conductor.

Based on the numerical method reported in [39], we numerically solve for the microscopic fields in ((4)) as $\beta\to 0$, then integrate these microscopic fields over a unit cell as shown in (13) and (20) to find $\mathbf{D}(0,k_0d)$ and $\mathbf{H}(0,k_0d)$ from (23), and finally determine $\overline{\boldsymbol{\epsilon}}(0,k_0d)$ and $\overline{\boldsymbol{\mu}}_{tt}(\boldsymbol{\beta}\to 0,k_0d)$ from (39) and (41). For propagation in the principal direction z of the array with the given applied electric current density in the $\hat{\mathrm{x}}$ direction, the vectors $\mathbf{E}(0,k_0d)$ and $\mathbf{D}(0,k_0d)$ are in the $\hat{\mathrm{x}}$ direction,

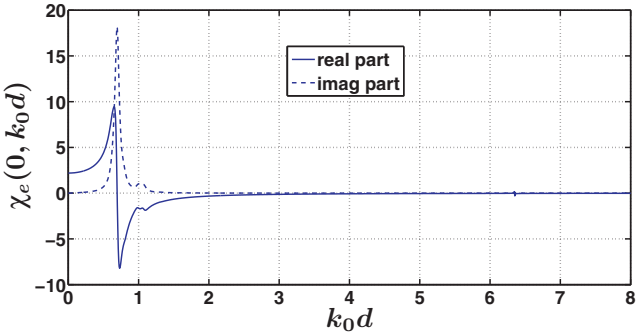

Fig. 1. Computed fundamental Floquet-mode macroscopic electric susceptibility for 2D array of dielectric circular cylinders ($a/d = 0.40$).

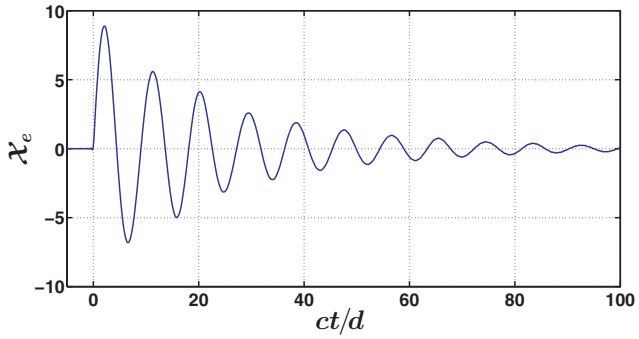

Fig. 3. Causality of numerically computed time-domain fundamental Floquet-mode electric susceptibility for 2D array of conductive dielectric circular cylinders ($a/d = 0.40$).

and the vectors $\mathbf{B}(0, k_0d)$ and $\mathbf{H}(0, k_0d)$ are in the $\hat{\mathbf{y}}$ direction (along the axis of the cylinders). Thus the permittivity and permeability reduce to scalars, $\epsilon(0, k_0d)$ and $\mu(0, k_0d)$, and the magnetoelectric dyadic $\overline{\boldsymbol{\nu}}_{tl} = 0$. As $\beta \to 0$ the only required integrations in (20) for the 2D cylinders reduce to

$$\mathbf{P}^e_\rho(0,\omega) = -\frac{1}{d^2}\int_{A_c} \nabla\cdot\boldsymbol{\mathcal{P}}_\omega(\mathbf{r})\mathbf{r}d^2r = \frac{1}{d^2}\int_{\text{cylinder}} \boldsymbol{\mathcal{P}}_\omega(\mathbf{r})d^2r \tag{82a}$$

for the electric polarization, and

$$\mathbf{M}^e(\beta\to 0,\omega) = -\frac{i\omega}{2d^2}\lim_{\beta\to 0}\int_{\text{cylinder}} \mathbf{r}\times\boldsymbol{\mathcal{P}}_\omega(\mathbf{r})e^{-i\beta z}d^2r \tag{82b}$$

for the magnetic polarization.

Fig. 1 shows the real and imaginary parts of the computed fundamental Floquet-mode macroscopic electric susceptibility $\chi_e(0, k_0d) = [\epsilon(0, k_0d)/\epsilon_0 - 1]$ versus the electrical separation distance k_0d. An enlargement of the second resonance region near $k_0d = 6.35$ is shown in Fig. 2. Each of the resonances

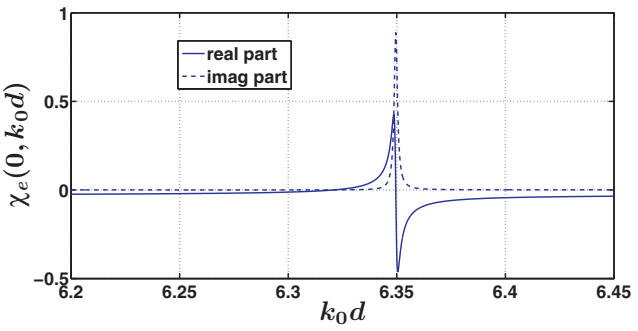

Fig. 2. Computed fundamental Floquet-mode macroscopic electric susceptibility for 2D array of dielectric circular cylinders ($a/d = 0.40$): enlargement of resonance near $k_0d = 6.35$.

resembles a Lorentz resonance. As predicted in Eq. (71c) the imaginary part of $\chi_e(0, k_0d)$ is greater than zero for $\omega > 0$ (that is, for $k_0d > 0$). The imaginary part remains quite small except near the resonances where it increases in value dramatically.

The real part of the electric susceptibility continuously increases from a positive value of about 2.2 at $k_0d = 0$ until it reaches the first resonance where it decreases rapidly to a negative value before increasing toward a value of zero and higher near the second resonance where the behavior is repeated. For $k_0d \ll 1$ the behavior of the real and imaginary parts of the fundamental Floquet-mode macroscopic electric susceptibility shown in Fig. 1 for the 2D array of conductive dielectric cylinders is similar to the behavior of the Clausius–Mossotti electric susceptibility shown in [5, fig. 8] for the 3D array of PEC spheres.

As determined by (77c), the fundamental Floquet-mode macroscopic permittivity and thus the macroscopic electric susceptibility of the 2D array of circular cylinders is a causal function satisfying

$$\mathcal{X}_e(\tau) = 2\text{Re}\int_0^{+\infty} \chi_e(0,k_0d)e^{-ik_0d\tau}d(k_0d) = 0 \tag{83}$$

for $\tau = ct/d < 0$. Fig. 3, which shows the plot of $\mathcal{X}_e(\tau)$ numerically computed from the integral in (83) using the $\chi_e(0, k_0d)$ data shown in Fig. 1, confirms the causality of this numerically computed electric susceptibility. (Using $\chi_e(0, k_0d)$ data for a maximum k_0d lying about half way between two resonances produces an effectively causal $\mathcal{X}_e(\tau)$.) Moreover, as discussed at the end of Section 4.4, since the macroscopic permittivity $\epsilon(0, k_0d)$ approaches 1 as $k_0d \to \infty$ and the imaginary part of $\epsilon(0, k_0d)$ is greater than zero for $k_0d > 0$, the theorem in the Appendix of [21] predicts that the inverse electric susceptibility defined

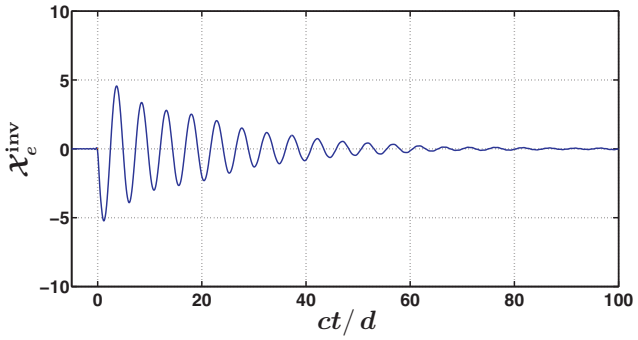

Fig. 4. Causality of numerically computed time-domain fundamental Floquet-mode *inverse* electric susceptibility for 2D array of conductive dielectric circular cylinders ($a/d = 0.40$).

as $\chi_e^{\mathrm{inv}}(0, k_0 d) = [\epsilon_0/\epsilon(0, k_0 d) - 1]$ is also a causal function; specifically

$$\mathcal{X}_e^{\mathrm{inv}}(\tau) = 2\mathrm{Re}\int_0^{+\infty} \chi_e^{\mathrm{inv}}(0, k_0 d) e^{-ik_0 d\tau} d(k_0 d) = 0 \tag{84}$$

for $\tau = ct/d < 0$. The causality of inverse electric susceptibility is confirmed numerically by computing the integral in (84) and plotting the results in Fig. 4.

Next, we show in Fig. 5 the real and imaginary parts of the computed fundamental Floquet-mode macroscopic magnetic susceptibility $\chi_m(0, k_0 d) = [\mu(0, k_0 d)/\mu_0 - 1]$ versus the electrical separation distance $k_0 d$. This $\chi_m(0, k_0 d)$ is computed from the magnetization in (82b) and the average (macroscopic) magnetic field $\mathbf{H}$ in the unit cell. As predicted by (73c), the imaginary part of the magnetic susceptibility is greater than zero for $k_0 d \ll 1$ and yet becomes less than zero at larger values of $k_0 d$ as a result of the resonant response of the inclusions.

The real part of the fundamental Floquet-mode macroscopic magnetic susceptibility is negative at the lower frequencies because the conductivity of the inclusion material produces a diamagnetic effect in this frequency range. (For the loss constant $k_c = 0$ in the Drude-model relative dielectric constant (81), the

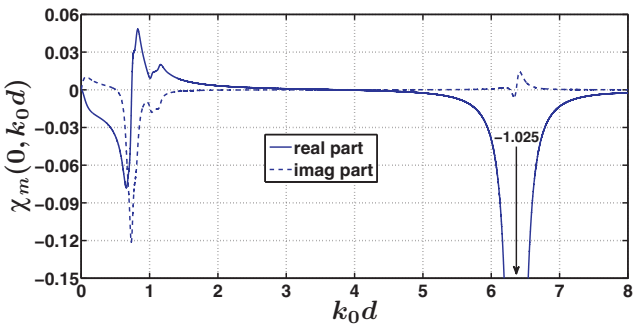

Fig. 5. Computed fundamental Floquet-mode macroscopic magnetic susceptibility for 2D array of dielectric circular cylinders ($a/d = 0.40$).

macroscopic magnetic susceptibility equals -0.0206 as $k_0 d \to 0$ and the macroscopic electric susceptibility equals 2.1944 as $k_0 d \to 0$.) The diamagnetism increases until the first resonance is reached where the real part rapidly increases to a positive value and stays positive until encountering the beginning of a second resonance at which the real part of the magnetic susceptibility becomes strongly diamagnetic again. The first resonance in the magnetic susceptibility approximates the negative of a Lorentz permittivity resonance. The second resonance shows very unusual behavior in that it somewhat imitates the negative of a Lorentz permittivity resonance but with the roles of the real and imaginary parts of the susceptibility reversed. For $k_0 d \ll 1$ the negative real and positive imaginary parts of the fundamental Floquet-mode macroscopic magnetic susceptibility shown in Fig. 5 for the 2D array of conductive dielectric cylinders is consistent with the negative real and positive imaginary parts of the Clausius–Mossotti magnetic susceptibility shown in [5, fig. 8] for the 3D array of PEC spheres. (Although not obvious from Fig. 5, the imaginary part of the susceptibility $\chi_m(0, k_0 d) \to 0$ as $k_0 d \to 0$.)

The theory of causality in Section 4.4 predicts in (77b) that the fundamental Floquet-mode macroscopic *inverse* permeability and thus the macroscopic inverse magnetic susceptibility defined as $\chi_m^{\mathrm{inv}}(0, k_0 d) = [\mu_0/\mu(0, k_0 d) - 1]$ for the 2D array of circular cylinders is a causal function satisfying

$$\mathcal{X}_m^{\mathrm{inv}}(\tau) = 2\mathrm{Re}\int_0^{+\infty} \chi_m^{\mathrm{inv}}(0, k_0 d) e^{-ik_0 d\tau} d(k_0 d) = 0 \tag{85}$$

for $\tau = ct/d < 0$. Fig. 6, which shows the plot of $\mathcal{X}_m^{\mathrm{inv}}(\tau)$ numerically computed from the integral in (85) using the $\chi_m(0, k_0 d)$ data shown in Fig. 5, confirms the causality of this numerically computed inverse magnetic susceptibility. (Using $\chi_m(0, k_0 d)$ data for a maximum $k_0 d$ lying about half way between two resonances produces an effectively causal $\mathcal{X}_m^{\mathrm{inv}}(\tau)$.) However, as discussed at the end of Section 4.4, since the imaginary part of $\mu(0, k_0 d)$, and thus $1/\mu(0, k_0 d)$, does not maintain the same sign for all $k_0 d > 0$, the theorem in the Appendix cannot be used to predict that the magnetic susceptibility $\chi_m(0, k_0 d)$ is a causal function. Indeed, the computation of

$$\mathcal{X}_m(\tau) = 2\mathrm{Re}\int_0^{+\infty} \chi_m(0, k_0 d) e^{-ik_0 d\tau} d(k_0 d) \tag{86}$$

plotted in Fig. 7 using the $\chi_m(0, k_0 d)$ data shown in Fig. 5 verifies that the fundamental Floquet-mode macroscopic magnetic susceptibility is definitely not causal.

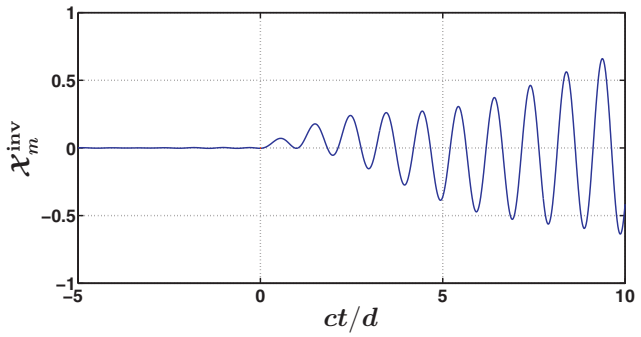

Fig. 6. Causality of numerically computed time-domain fundamental Floquet-mode *inverse* magnetic susceptibility for 2D array of conductive dielectric circular cylinders ($a/d = 0.40$).

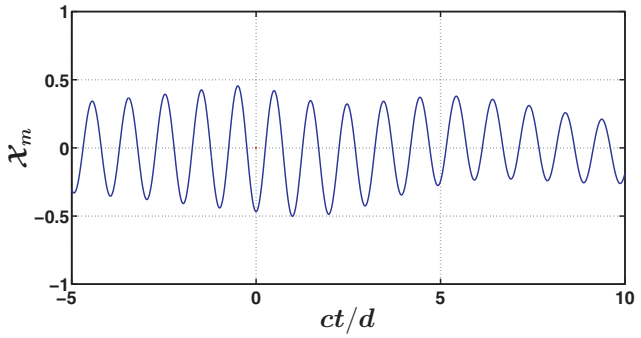

Fig. 7. Noncausality of numerically computed time-domain fundamental Floquet-mode magnetic susceptibility for 2D array of conductive dielectric circular cylinders ($a/d = 0.40$).

6. Conclusion

At high enough frequencies ω, every natural material or artificial material (metamaterial) no longer behaves as a continuum satisfying the traditional time-harmonic dipolar macroscopic Maxwell equations with spatially nondispersive constitutive parameters. Although this departure from a continuum behavior at high frequencies can often be ignored with impunity for the electric and para/ferro(i)magnetic polarization of materials and metamaterials, we show in Section 1 that it is mathematically impossible to characterize a material or metamaterial that is diamagnetic and lossless at low frequencies ω by a causal spatially nondispersive permeability that satisfies continuum passivity conditions and whose value approaches the permeability of free space as the frequency ω approaches infinity. Moreover, this noncausality in the spatially nondispersive dipolar continuum description of diamagnetism is more fundamental than the noncausality, discussed in [20], introduced by the point dipole approximation for scattering from the inclusions (molecules) and is not removed by including higher-order multipole moments in the spatially nondispersive continuum formulation of Maxwell's equations.

In order to characterize metamaterials formed by periodic arrays of polarizable inclusions (separated in free space) in a way that includes diamagnetism and reduces to a continuum description when the enforced and free-space wavelengths in the arrays are large compared to the distance separating the inclusions, we formulate a rigorous spatially ($\boldsymbol{\beta}$) and temporally (ω) dispersive anisotropic representation for these periodic metamaterials. The spatially dispersive anisotropic representation, like the single-polarization description of materials introduced by Landau and Lifshitz [2], is obtained by exciting the metamaterial arrays with applied electric current densities having $e^{i(\boldsymbol{\beta}\cdot\mathbf{r}-\omega t)}$ plane-wave dependence. Beginning with the microscopic Maxwell's equations for the arrays, it is shown that two constitutive parameters, a spatially dispersive permittivity $\overline{\boldsymbol{\epsilon}}(\boldsymbol{\beta},\omega)$ and a spatially dispersive *inverse* transverse permeability $\overline{\boldsymbol{\mu}}_{tt}^{-1}(\boldsymbol{\beta},\omega)$, characterize the fundamental Floquet modes of the arrays. These macroscopic permittivities and inverse permeabilities are shown to be causal for each fixed value of the plane-wave propagation vector $\boldsymbol{\beta}$ and to reduce to continuum permittivities and permeabilities at the low spatial and temporal frequencies ($|\boldsymbol{\beta}d|$ and $|k_0 d|$ sufficiently small). The general formulation for spatially dispersive periodic arrays provides convenient equations to express sufficient conditions for the array to approximate a continuum, and to determine boundary conditions for an electric quadrupolar continuum.

The key to this rigorous spatially dispersive anisotropic formulation is the vector decomposition given in (17) for the microscopic equivalent electric current density and the resulting generalized dipolar and electric quadrupolar macroscopic polarization densities in (20). For both $|\boldsymbol{\beta}d|$ and $|k_0 d|$ sufficiently small, the array behaves as an anisotropic dipolar continuum in which the electric quadrupolar density, and all other higher-order multipoles, are negligible compared with a nonzero dipolar electric and/or magnetic polarization density. This result for an anisotropic continuum is a significant consequence of the rigorous anisotropic representation for spatially dispersive media.

Detailed reality conditions, reciprocity relations, passivity conditions, and causality relations are derived for the macroscopic anisotropic permittivities and permeabilities. Some unusual results emerge from these derivations. Except at the low spatial and temporal frequencies where arrays generally behave as dipolar continua, the reciprocity relations and

passivity conditions satisfied by the permittivities and permeabilities are coupled. In particular, the imaginary parts of the diagonal elements of the macroscopic permittivities and permeabilities need not be equal to or greater than zero even though the power dissipated by the passive inclusions is always equal to or greater than zero. This curious result remains true for a diamagnetic permeability even as the spatial propagation constant $\boldsymbol{\beta}$ approaches zero. It is the main reason for the nonexistence of a causal, spatially *nondispersive*, inverse diamagnetic (at low frequencies) permeability that satisfies the usual continuum passivity condition (imaginary parts of the diagonal elements equal to or less than zero), and approaches μ_0^{-1} as $|\omega| \to \infty$.

We also find the rather unusual theoretical result that the spatially dispersive permeability for the fundamental Floquet mode, unlike the inverse permeability for the fundamental Floquet mode, need not satisfy causality. This result stems from the necessity to use the $\boldsymbol{\mathcal{E}}$ and $\boldsymbol{\mathcal{B}}$ vectors as the primary microscopic fields in the formulation of Maxwell's macroscopic equations for electric charge-current definitions of electric and magnetic polarization.

The anisotropic theory of spatially dispersive periodic arrays is reinforced with a numerical example. We solve the derived equations for a 2D periodic array of circular cylinders with Drude-model dielectric inclusions. For a fixed $\boldsymbol{\beta} \to 0$, the computed macroscopic permittivity and permeability confirms the theoretical predictions that the imaginary part of the fundamental Floquet-mode permittivity as $\boldsymbol{\beta} \to 0$ satisfies the usual continuum passivity condition of being equal to or greater than zero for all ω, whereas the imaginary part of the fundamental Floquet-mode permeability as $\boldsymbol{\beta} \to 0$ satisfies the usual continuum passivity condition only at the lower frequencies but becomes negative at the higher values of ω. Moreover, we confirm that the fundamental Floquet-mode permittivity and fundamental Floquet-mode inverse permittivity satisfy causality and the Kramers–Kronig relations. In contrast, while the fundamental Floquet-mode inverse permeability satisfies causality and the Kramers–Kronig relations, the fundamental Floquet-mode permeability itself does not satisfy causality—a result that further substantiates the theory.

Acknowledgement

This research was supported in part under the U.S. Air Force Office of Scientific Research (AFOSR) grant FA9550-12-1-0105 through Dr. A. Nachman.

References

[1] T.B. Hansen, A.D. Yaghjian, Plane-Wave Theory of Time-Domain Fields: Near-Field Scanning Applications, IEEE/Wiley Press, Piscataway, NJ, 1999.
[2] L.D. Landau, E.M. Lifshitz, L.P. Pitaevskii, Electrodynamics of Continuous Media, 2nd ed., Butterworth Heinemann, Oxford, 1984
[3] A.D. Yaghjian, Internal energy, Q-energy, Poynting's theorem, and the stress dyadic in dispersive material, IEEE Transactions on Antennas and Propagation 55 (2007) 1495–1505, Correction 55:3748.
[4] H.A. Haus, J.R. Melcher, Electromagnetic Fields and Energy, Prentice Hall, Englewood Cliffs, NJ, 1989.
[5] R.A. Shore, A.D. Yaghjian, Traveling waves on two- and three-dimensional periodic arrays of lossless scatterers, Radio Science 42 (2008) RS6S21, Correction 43:RS2S99.
[6] M.G. Silveirinha, Examining the validity of the Kramers–Kronig relations for the magnetic permeability, Physical Review B 83 (2011) 165119.
[7] D.R. Smith, J.B. Pendry, Homogenization of metamaterials by field averaging, Journal of the Optical Society of America B 23 (2006) 391.
[8] I. Tsukerman, Effective parameters of metamaterials: a rigorous homogenization theory via Whitney interpolation, Journal of the Optical Society of America B 28 (2011) 577.
[9] A.P. Vinogradov, A.V. Aivazyan, Scaling theory for homogenization of the Maxwell equations, Physical Review E 60 (1999) 987.
[10] A. Andryieuski, S. Ha, A.A. Sukhorukov, Y.S. Kivshar, A.V. Lavrinenko, Bloch-mode analysis for retrieving effective parameters of metamaterials, Physical Review B 86 (2012) 035127.
[11] V.P. Silin, A.A. Rukhadze, Electromagnetic Properties of Plasmas and Plasma-Like Media, Gosatomizdat, Moscow, 1961 (in Russian).
[12] V.M. Agranovich, V.L. Ginzburg, Spatial Dispersion in Crystal Optics and the Theory of Excitons, Wiley-Interscience, New York, 1966, also see 2nd ed. (1984), Springer-Verlag, New York.
[13] M.G. Silveirinha, Nonlocal homogenization theory of structured materials, in: F. Capolino (Ed.), Metamaterials Handbook: Theory and Phenomena of Metamaterials, CRC Press, Boca Raton, FL, 2009 (Chapter 10).
[14] M.G. Silveirinha, Metamaterial homogenization approach with application to the characterization of microstructured composites with negative parameters, Physical Review B 75 (2007) 115104.
[15] M.G. Silveirinha, Time domain homogenization of metamaterials, Physical Review B 83 (2011) 165104.
[16] C. Fietz, G. Shvets, Current-driven metamaterial homogenization, Physica B 405 (2010) 2930.
[17] M.G. Silveirinha, Generalized Lorentz–Lorenz formulas for microstructured materials, Physical Review B 76 (2007) 245117.
[18] A. Alù, First-principles homogenization theory for periodic metamaterial arrays, Physical Review B 84 (2011) 075153.
[19] J.A. Kong, Electromagnetic Wave Theory, Wiley Press, New York, 1986.
[20] A. Alù, A.D. Yaghjian, R.A. Shore, M.G. Silveirinha, Causality relations in the homogenization of metamaterials, Physical Review B 84 (2011) 054305.
[21] A.D. Yaghjian, A. Alù, M.G. Silveirinha, Anisotropic representation for spatially dispersive periodic metamaterial arrays, in: D.H. Werner, D.-H. Kwon (Eds.), Transformation Electromagnetics and Metamaterials: Fundamental Principles and Applications, Springer, New York, 2013.

[22] J.A. Stratton, Electromagnetic Theory, McGraw-Hill, New York, 1941.
[23] R.A. Shore, A.D. Yaghjian, Complex waves on periodic arrays of lossy and lossless permeable spheres: 1. Theory; and 2. Numerical results, Radio Science 47 (2012) RS2014, 47:RS2015.
[24] R.E. Raab, O.L. De Lange, Multipole Theory in Electromagnetism, Clarendon, Oxford, 2005.
[25] C.H. Papas, Theory of Electromagneic Wave Propagation, McGraw-Hill, New York, 1965 (Dover 1988).
[26] F.N.H. Robinson, Macroscopic Electromagnetism, Pergamon Press, Oxford, 1973.
[27] W.T. Scott, The Physics of Electricity and Magnetism, 2nd ed., Robert E. Krieger, Huntington, NY, 1977.
[28] M.G. Silveirinha, Poynting vector, heating rate, and stored energy in structured materials: a first-principles derivation, Physical Review B 80 (2009) 235120.
[29] M.G. Silveirinha, J.T. Costa, A. Alù, Poynting vector in negative-index metamaterials, Physical Review B 83 (2011) 165120.
[30] P. Drude, The Theory of Optics, Longmans, Green, New York, 1902, Dover (2005).
[31] A.D. Yaghjian, Extreme electromagnetic boundary conditions and their manifestation at the inner surfaces of spherical and cylindrical cloaks, Metamaterials 4 (2010) 70.
[32] M.G. Silveirinha, C.A. Fernandes, Transverse-average field approach for the characterization of thin metamaterial slabs, Physical Review E 75 (2007) 036613.
[33] C.R. Simovski, S.A. Tretyakov, Local constitutive parameters of metamaterials from an effective-medium perspective, Physical Review B 75 (2007) 195111.
[34] A.D. Scher, E.F. Kuester, Boundary effects in the electromagnetic response of a metamaterial in the case of normal incidence, PIER B 14 (2007) 341.
[35] V.M. Agranovich, Y.R. Shen, R.H. Baughman, A.A. Zakhidov, Linear and nonlinear wave propagation in negative refraction metamaterials, Physical Review B 69 (2004) 165112.
[36] L. Mirsky, An Introduction to Linear Algebra, Oxford University Press, Oxford, 1955.
[37] C.R. Simovsky, Analytical-modeling of double-negative composites, Metamaterials 2 (2008) 169.
[38] J.K. Lu, Boundary Value Problems for Analytical Functions, World Scientific, New York, 1993.
[39] J.T. Costa, M.G. Silveirinha, S.I. Maslovski, Finite-difference frequency-domain method for the extraction of the effective parameters of metamaterials, Physical Review B 80 (2009) 235124.